

Nonlinear stratified spin-up

By LEIF N. THOMAS AND PETER B. RHINES

School of Oceanography, University of Washington, Box 355351,
Seattle, Washington 98195-5351, USA
leif@ocean.washington.edu; rhines@ocean.washington.edu

(Received 20 December 2000 and in revised form 24 June 2002)

Both a weakly nonlinear analytic theory and direct numerical simulation are used to document processes involved during the spin-up of a rotating stratified fluid driven by wind-stress forcing for time periods less than a homogeneous spin-up time. The strength of the wind forcing, characterized by the Rossby number ϵ , is small enough (i.e. $\epsilon \ll 1$) that a regular perturbation expansion in ϵ can be performed yet large enough (more specifically, $\epsilon \propto E^{1/2}$, where E is the Ekman number) that higher-order effects of vertical diffusion and horizontal advection of momentum/density are comparable in magnitude. Cases of strong stratification, where the Burger number S is equal to one, with zero heat flux at the upper boundary are considered. The Ekman transport calculated to $O(\epsilon)$ decreases with increasing absolute vorticity. In contrast to nonlinear barotropic spin-up, vortex stretching in the interior is predominantly linear, as vertical advection negates stretching of interior relative vorticity, yet is driven by Ekman pumping modified by nonlinearity. As vertical vorticity is generated during the spin-up of the fluid, the vertical vorticity feeds back on the Ekman pumping/suction, enhancing pumping and vortex squashing while reducing suction and vortex stretching. This feedback mechanism causes anticyclonic vorticity to grow more rapidly than cyclonic vorticity. Strict application of the zero-heat-flux boundary condition leads to the growth of a diffusive thermal boundary layer $E^{-1/4}$ times thicker than the Ekman layer embedded within it. In the Ekman layer, vertical diffusion of heat balances horizontal advection of temperature by extracting heat from the thermal boundary layer beneath. The flux of heat extracted from the top of the thermal boundary layer by this mechanism is proportional to the product of the Ekman transport and the horizontal gradient of the temperature at the surface. The cooling caused by this heat flux generates density inversions and intensifies lateral density gradients where the wind-stress curl is negative. These thermal gradients make the potential vorticity strongly negative, conditioning the fluid for ensuing symmetric instability which greatly modifies the spin-up process.

1. Introduction

Apart from buoyancy forcing, the major driving force for motions within the ocean is the wind stress. Conversely, surface stress at the base of the atmosphere provides the major retarding force for its circulation. In the presence of rotation, boundary stress will drive, within the turbulent boundary layer, a net mass transport at right angles to the stress. Divergences and convergences of this Ekman transport will result if the surface stress has a curl. These divergences (convergences) pump fluid out of (into) the interior of the fluid, setting up a secondary circulation. Despite the weakness of this circulation, it has major consequences on the flow because of rotation

and stratification. Due to the Coriolis force, the horizontal motions associated with this circulation will continually accelerate a flow perpendicular to the secondary circulation, while the vertical motions will advect the density field. This accelerative process, termed stratified spin-up (SSU), is fundamental to geophysical flows and has been studied extensively (Holton 1965*a, b*; Sakurai 1969; Walin 1969; Buzyna & Veronis 1971; Allen 1973). Common to all of these analyses is the assumption that the magnitude of the flow induced by this process is small enough so that nonlinear advection of momentum and density is negligible, i.e. that the Rossby number $\epsilon = U/(fL)$ (where U and L are scales for the magnitude and length of the flow and f is the Coriolis parameter) is very small. For the case of the ocean forced by a wind-stress curl constant in time, SSU generates interior-geostrophic flow in the direction of the wind that grows linearly with time (Allen 1973). Hence, with such forcing, the Rossby number continually increases, and at some time advection of momentum and density by the secondary circulation cannot be neglected from the dynamics of SSU. The assumption of linear dynamics of SSU theory then comes into question. Previous theories of SSU fail to properly account for flux boundary conditions on the density field at the top and bottom of the fluid. In this paper we use a zero-heat-flux boundary condition so as to put the emphasis on mechanical versus buoyancy-driven dynamics. We will show that correct application of zero-heat-flux boundary conditions is crucial to both the thermodynamics and the dynamics of the flow near the surface, for inversions and front-like features are manifested in the density field, confounding the assumption of laminar hydrostatic nearly geostrophic surface flow.

Since the secondary circulation is strongest in the Ekman layer, that is where nonlinear effects should be intensified. How does advection of momentum modify the dynamics in the Ekman layer? Although this issue has not been addressed in the context of SSU, Stern (1965) and Niiler (1969) considered the nonlinear interaction between the Ekman flow and a pre-existing geostrophic vortex and barotropic current respectively. The approach of Stern was to use scale analysis, whereas Niiler explicitly solved for the linearized wind-driven flow about a barotropic ocean current. Both studies focused on the vertically integrated response of the flow in the Ekman layer, concluding that the Ekman transport induced by a wind stress τ blowing in the direction of the pre-existing flow is given by

$$M_{nl} = \frac{\tau}{\rho(f + \zeta)}, \quad (1.1)$$

where ρ is the density, f is the Coriolis parameter, and ζ is the vertical component of the relative vorticity associated with the pre-existing flow. Thus, for flows where the Rossby number is significant, the Ekman transport varies inversely with the absolute vorticity $f + \zeta$ rather than planetary vorticity f . The most striking consequence of this result is that Ekman pumping/suction

$$w_{nl} = \frac{1}{\rho(f + \zeta)} \frac{\partial \tau}{\partial x} - \frac{\tau}{\rho(f + \zeta)^2} \frac{\partial \zeta}{\partial x} \quad (1.2)$$

(where x is the coordinate perpendicular to the flow as well as the wind) can occur even if the wind stress does not have a curl, as a result of spatial variations in the vertical vorticity, i.e. the second term of (1.2). Generation of Ekman pumping by a spatially uniform wind stress was investigated numerically in the study of Lee *et al.* (1994), in which such a wind was applied to an oceanic current initially in geostrophic balance. In contrast, our study uses a spatially varying wind stress, and hence both

the first term in (1.2), which implies that Ekman pumping induced by the curl of the wind stress is amplified (reduced) in regions of anticyclonic (cyclonic) vorticity, and the second term in (1.2) will be active in the dynamics.

The dependence of the Ekman pumping on the vertical vorticity presents a coupling between the Ekman layer and the flow in the interior of the ocean. We investigate the effects of this coupling, horizontal advection of density by the Ekman flow, and the vertical diffusion of density on the spin-up of a stratified fluid forced by a wind stress varying sinusoidally in the direction perpendicular to the wind. This forcing is used to highlight the fundamental differences between linear and nonlinear SSU. The nonlinear analysis is accomplished by the use of a regular perturbation expansion in orders of the Rossby number for all the flow variables. An analytical expression for the second-order flow in the Ekman layer is calculated, from which its dependence on the parameters involved (stratification, rotation, wind stress strength and length scale) and the new features which nonlinearities bring to the solution (sharpening of gradients, asymmetries, etc.) are determined explicitly. The pumping/suction induced by the second-order flow is then used to drive a secondary circulation in the interior whose effect is to accelerate a flow parallel to the wind. A solution for the density field is derived which accounts for the no-heat-flux boundary conditions, horizontal and vertical advection of density by the Ekman flow, and the distortion of interior vertical advection by the second-order flow. A numerical experiment using a fully nonlinear two-dimensional non-hydrostatic numerical model is performed to explore the validity of, as well as extend, the analytical solution.

The outline of the paper is as follows. First, the formulation of the SSU problem and description of the numerical model are given. Next, the details and failures of classic SSU theory are presented in §3. Following this, the method and solution of the weakly nonlinear theory of SSU is described in §4. The paper is concluded with a discussion in §5.

2. Formulation

2.1. Basic equations

The basic equations governing motion of an incompressible Boussinesq fluid on an f -plane rotating about the vertical axis with an angular velocity of $\Omega = f/2$ are

$$\nabla \cdot \mathbf{q} = 0, \quad (2.1)$$

$$\frac{\partial \mathbf{q}}{\partial t} + \mathbf{q} \cdot \nabla \mathbf{q} + f \hat{\mathbf{k}} \times \mathbf{q} = \frac{-\nabla p}{\rho_o} - \frac{\rho}{\rho_o} g \hat{\mathbf{k}} + \kappa \nabla^2 \mathbf{q}, \quad (2.2)$$

$$\frac{\partial T}{\partial t} + \mathbf{q} \cdot \nabla T = \kappa^d \nabla^2 T, \quad (2.3)$$

$$\rho = \rho_o(1 - \alpha(T - T_o)), \quad (2.4)$$

where $\mathbf{q} = (u, v, w)$, p , ρ and T are respectively the velocity, pressure, density and temperature of the fluid. We assume that the fields are invariant in one lateral direction so all variables are only functions of the horizontal and vertical position (x, z) as well as the time t . The diffusivities of momentum and heat are denoted by κ and κ^d respectively, and $-g\hat{\mathbf{k}}$ is the gravitational acceleration with $\hat{\mathbf{k}}$ indicating the vertical unit vector. The linearized equation of state of the fluid is given in (2.4) with α being the thermal expansion coefficient, and ρ_o indicating the density at a reference temperature T_o .

We assume the undisturbed fluid to have a uniform stable stratification: $T_b = \Delta T(z/H) + T_o$ with buoyancy frequency $N = \sqrt{\alpha g \Delta T / H}$, where ΔT is the background temperature difference imposed across the fluid depth H .

The equations are non-dimensionalized by scaling the variables in the following way:

$$\begin{aligned} x &= Lx', & z &= Hz', & t &= \tau_h t', \\ u &= Uu', & v &= Uv', & w &= (UH/L)w', \\ p &= p_b + (UfL\rho_o)p', & T &= \Delta T[z/H + (\epsilon/S)T'], \end{aligned}$$

where L is a characteristic horizontal length scale, U is a characteristic horizontal velocity, p_b is the hydrostatic background pressure associated with the background temperature field, $\epsilon = U/(fL)$ is the Rossby number and $S = N^2 H^2 / (f^2 L^2)$ is the Burger number representing the ratio of the square of the Rossby radius of deformation $L_r = NH/f$ to the square of the characteristic length scale L . Following earlier work on stratified spin-up (Sakurai 1969; Buzyna & Veronis 1971; Allen 1973), we scale time in terms of the spin-up time of a homogeneous fluid $\tau_h = E^{-1/2} f^{-1}$ (Greenspan & Howard 1963), where $E = 2\kappa / (fH^2)$ is the Ekman number. This change of variable effectively filters out inertial oscillations as well as the temporal development of the flow in the Ekman layer, processes which occur over an inertial period (i.e. $\tau_i = 2\pi f^{-1}$) and which are not the focus of this study, but will nonetheless appear in the numerical simulation.

The motion of the fluid is driven by a wind stress τ with a magnitude τ_o applied at the surface in the y -direction. It is anticipated that this wind stress will induce an Ekman transport to the right of itself with a magnitude $M = \tau_o / (\rho_o f)$. This transport is distributed across the thickness of the Ekman layer $\delta_e = \sqrt{2\kappa / f}$. Knowing this we can estimate the characteristic horizontal velocity to be $U = \tau_o / (\rho_o f \delta_e)$.

The dimensionless equations are (dropping the primes):

$$\frac{\partial u}{\partial x} + \frac{\partial w}{\partial z} = 0, \quad (2.5)$$

$$E^{1/2} \frac{\partial u}{\partial t} + \epsilon \left(u \frac{\partial u}{\partial x} + w \frac{\partial u}{\partial z} \right) - v = -\frac{\partial p}{\partial x} + \frac{E}{2} \left(\frac{\partial^2 u}{\partial z^2} + \frac{1}{\Gamma} \frac{\partial^2 u}{\partial x^2} \right), \quad (2.6)$$

$$E^{1/2} \frac{\partial v}{\partial t} + \epsilon \left(u \frac{\partial v}{\partial x} + w \frac{\partial v}{\partial z} \right) + u = \frac{E}{2} \left(\frac{\partial^2 v}{\partial z^2} + \frac{1}{\Gamma} \frac{\partial^2 v}{\partial x^2} \right), \quad (2.7)$$

$$E^{1/2} \frac{\partial w}{\partial t} + \epsilon \left(u \frac{\partial w}{\partial x} + w \frac{\partial w}{\partial z} \right) = \Gamma \left(-\frac{\partial p}{\partial z} + T \right) + \frac{E}{2} \left(\frac{\partial^2 w}{\partial z^2} + \frac{1}{\Gamma} \frac{\partial^2 w}{\partial x^2} \right), \quad (2.8)$$

$$E^{1/2} \frac{\partial T}{\partial t} + \epsilon \left(u \frac{\partial T}{\partial x} + w \frac{\partial T}{\partial z} \right) + Sw = \frac{E}{2\sigma} \left(\frac{\partial^2 T}{\partial z^2} + \frac{1}{\Gamma} \frac{\partial^2 T}{\partial x^2} \right), \quad (2.9)$$

where $\Gamma = (L/H)^2$ is the square of the aspect ratio and $\sigma = \kappa / \kappa^d$ is the Prandtl number.

2.2. Boundary conditions, initial conditions, and forcing

The fluid is unbounded in the x -direction and is capped at $z = 1$ with a thermally insulated rigid boundary along which the wind stress is applied. The bottom boundary at $z = 0$ is an insulated no-slip wall. At $t = 0$ the wind stress is turned on impulsively.

This leads to the following boundary conditions on the dimensionless variables:

$$u = v = w = 0 \quad \text{at} \quad z = 0, \quad (2.10)$$

$$1 + \frac{\epsilon}{S} \frac{\partial T}{\partial z} = 0 \quad \text{at} \quad z = 0, 1, \quad (2.11)$$

$$w = \frac{\partial u}{\partial z} = 0, \quad \frac{\partial v}{\partial z} = 2E^{-1/2}\tau \quad \text{at} \quad z = 1 \quad (t > 0). \quad (2.12)$$

The form of the boundary condition for the temperature (2.11) ensures that the sum of the heat flux due to the background stratification and the temperature perturbation is zero at the horizontal boundaries.

We investigate the response of an initially motionless uniformly stratified rotating fluid to a wind stress that varies sinusoidally in the x -direction. The wavelength of this sinusoid is the characteristic length L . The initial conditions and form of the wind stress are as follows:

$$u = v = w = T = 0 \quad \text{at} \quad t = 0, \quad (2.13)$$

$$\tau = \cos(2\pi x). \quad (2.14)$$

We are interested in how nonlinear advection of momentum and temperature affect the spin-up of the fluid. Because of this, we consider cases where the Rossby number of the wind-driven flow ϵ is small yet large enough so that the effects of vertical diffusion and horizontal advection of momentum/density are comparable in magnitude. More specifically we assume that:

$$E^{1/2} = \gamma\epsilon, \quad (2.15)$$

$$\Gamma \gg 1, \quad (2.16)$$

$$S \sim 1, \quad (2.17)$$

$$\sigma = 1, \quad (2.18)$$

where γ is a proportionality constant of order-one. We restrict our analysis to time-scales of order a homogeneous spin-up time, i.e. $t = O(1)$.

2.3. Numerical model

Once the analytical solution using the above-mentioned approximations is found, we will explore its validity using a nonlinear two-dimensional non-hydrostatic numerical model. The model integrates the following equations forward in time:

$$\frac{\partial v}{\partial t} + u \frac{\partial v}{\partial x} + w \frac{\partial v}{\partial z} + f u = \kappa_v \frac{\partial^2 v}{\partial z^2} + \kappa_h \frac{\partial^2 v}{\partial x^2}, \quad (2.19)$$

$$\frac{\partial T}{\partial t} + u \frac{\partial T}{\partial x} + w \frac{\partial T}{\partial z} = \frac{1}{\sigma} \left(\kappa_v \frac{\partial^2 T}{\partial z^2} + \kappa_h \frac{\partial^2 T}{\partial x^2} \right), \quad (2.20)$$

$$\frac{\partial \chi}{\partial t} + u \frac{\partial \chi}{\partial x} + w \frac{\partial \chi}{\partial z} = f \frac{\partial v}{\partial z} - g\alpha \frac{\partial T}{\partial x} + \kappa_v \frac{\partial^2 \chi}{\partial z^2} + \kappa_h \frac{\partial^2 \chi}{\partial x^2}, \quad (2.21)$$

where $u = \partial\psi/\partial z$, $w = -\partial\psi/\partial x$, ψ is a stream function, and $\chi = \nabla^2\psi$ is the y -component of the vorticity. The notation used in the equations above is the same as that used previously in the text, apart from the vertical and horizontal diffusivities

L (m)	5.0×10^4
H (m)	1.0×10^3
τ_0 (N m ⁻²)	1.0×10^{-1}
N (s ⁻¹)	5.0×10^{-3}
f (s ⁻¹)	1.0×10^{-4}
κ_v (m ² s ⁻¹)	5.0×10^{-3}
κ_h (m ² s ⁻¹)	5.0
σ	1.0
ϵ	2.0×10^{-2}
S	1.0
E	1.0×10^{-4}

TABLE 1. The physical and non-dimensional parameters used in the numerical experiment and the analytical solution.

of momentum, κ_v and κ_h respectively, which are not necessarily the same in the numerical model. The physical and non-dimensional parameters used in the numerical experiment are listed in table 1.

The model uses a staggered grid with the temperature and the y -component of the velocity defined at the centre of the grid, u and w defined at the centre of the vertical and horizontal sides of the grid respectively, and χ at the corners of the grid. The horizontal and vertical grid spacing were $\Delta x = 100$ m and $\Delta z = 3.9$ m respectively. The vertical grid spacing was designed to be fine enough to resolve the Ekman layers. Boundary conditions on the upper and lower surfaces are the dimensional form of (2.10), (2.11) and (2.12). The width of the domain is equal to the wavelength of the wind forcing, i.e. L , and at $x = -L/2$ and $x = L/2$ the boundary conditions are periodic.

3. Linear stratified spin-up

3.1. Classical stratified spin-up theory

We now summarize the stress-driven stratified spin-up theory of Allen (1973) in which the assumptions $\epsilon = 0$ and $E \ll 1$ were used. Within an inertial period, wind stress applied at the surface generates cross-wind and vertical flow in a thin Ekman layer. The equations governing this flow are

$$\frac{1}{2} \frac{\partial^2 u_e}{\partial \eta^2} + v_e = 0, \quad (3.1)$$

$$\frac{1}{2} \frac{\partial^2 v_e}{\partial \eta^2} - u_e = 0, \quad (3.2)$$

where $\eta = (1 - z)/E^{1/2}$ is the stretched vertical coordinate in the Ekman layer near $z = 1$ and the subscript e denotes an Ekman-layer variable. The solution to (3.1) and (3.2) subject to the boundary conditions $\partial v_e / \partial \eta = -2 \cos(2\pi x)$ and $\partial u_e / \partial \eta = 0$, as represented by a stream function is

$$\psi_e = e^{-\eta} \cos(\eta) \cos(2\pi x), \quad (3.3)$$

where the stream function is related to the cross-wind and vertical velocities by

$$(u_e, w_e) = (-\partial \psi_e / \partial \eta, -E^{1/2} \partial \psi_e / \partial x). \quad (3.4)$$

Convergence (divergence) of the cross-wind flow pumps fluid into (out of) the interior of the fluid, outside the Ekman layer. This sets up an interior secondary circulation in the (x, z) -plane

$$(u_i, w_i) = E^{1/2}(\partial\psi_i/\partial z, -\partial\psi_i/\partial x) \quad (3.5)$$

(subscript i denotes an interior flow quantity) of strength $O(E^{1/2})$. Setting $\epsilon = 0$, collecting terms in equations (2.6)–(2.9) of like order in Ekman number, and utilizing (2.16) yields the equations governing the interior-flow variables:

$$\frac{\partial v_i}{\partial z} - \frac{\partial T_i}{\partial x} = 0, \quad (3.6)$$

$$\frac{\partial v_i}{\partial t} + \frac{\partial \psi_i}{\partial z} = 0, \quad (3.7)$$

$$\frac{\partial T_i}{\partial t} - S \frac{\partial \psi_i}{\partial x} = 0. \quad (3.8)$$

Eliminating v_i and T_i yields the following equation for ψ_i :

$$\frac{\partial^2 \psi_i}{\partial z^2} + S \frac{\partial^2 \psi_i}{\partial x^2} = 0. \quad (3.9)$$

The no-normal-flow conditions (2.10) and (2.12) set the boundary conditions for ψ_i :

$$\psi_i = -\psi_e \quad \text{at} \quad z = 1, \quad (3.10)$$

$$\frac{\partial \psi_i}{\partial t} = \frac{1}{2} \frac{\partial \psi_i}{\partial z} \quad \text{at} \quad z = 0. \quad (3.11)$$

The solution to (3.9) subject to (3.10) and (3.11), as derived by Allen (1973) is

$$\psi_i = - \left\{ \frac{\sinh(\lambda z)}{\sinh(\lambda)} e^{-\beta t} + \frac{\cosh(\lambda z)}{\cosh(\lambda)} [1 - e^{-\beta t}] \right\} \cos(2\pi x) \quad (3.12)$$

with $\lambda = 2\pi\sqrt{S}$ and $\beta = \lambda \coth(\lambda)/2$. Note that because of the constraining effects of stratification, this $O(E^{1/2})$ secondary circulation is concentrated near the surface in a layer of order a Prandtl depth, $\delta_s = H/\lambda$, thick. Integrating (3.7) and (3.8) and using the initial conditions (2.13), the solutions for v_i and T_i are

$$v_i = \lambda \left\{ \frac{\cosh(\lambda z)}{\beta \sinh(\lambda)} [1 - e^{-\beta t}] + \frac{\sinh(\lambda z)}{\cosh(\lambda)} \left[t - \frac{1}{\beta} [1 - e^{-\beta t}] \right] \right\} \cos(2\pi x), \quad (3.13)$$

$$T_i = 2\pi S \left\{ \frac{\sinh(\lambda z)}{\beta \sinh(\lambda)} [1 - e^{-\beta t}] + \frac{\cosh(\lambda z)}{\cosh(\lambda)} \left[t - \frac{1}{\beta} [1 - e^{-\beta t}] \right] \right\} \sin(2\pi x). \quad (3.14)$$

A crucial feature of these solutions is that they have terms which grow linearly with t . As a consequence of this secular growth, at some time the effects of advection of momentum and density by the secondary circulation will not be negligibly small, at which point these linear solutions will fail to accurately describe the SSU process.

3.2. Shortcomings of classical stratified spin-up theory

To obtain a qualitative sense of the limitations of classical stratified spin-up theory, we contrast the classical SSU solutions for the temperature, stream function, and downwind velocity near the surface with those from the numerical simulation (figures 1 and 2). The parameters used in the numerical simulation are listed in table 1. Both the

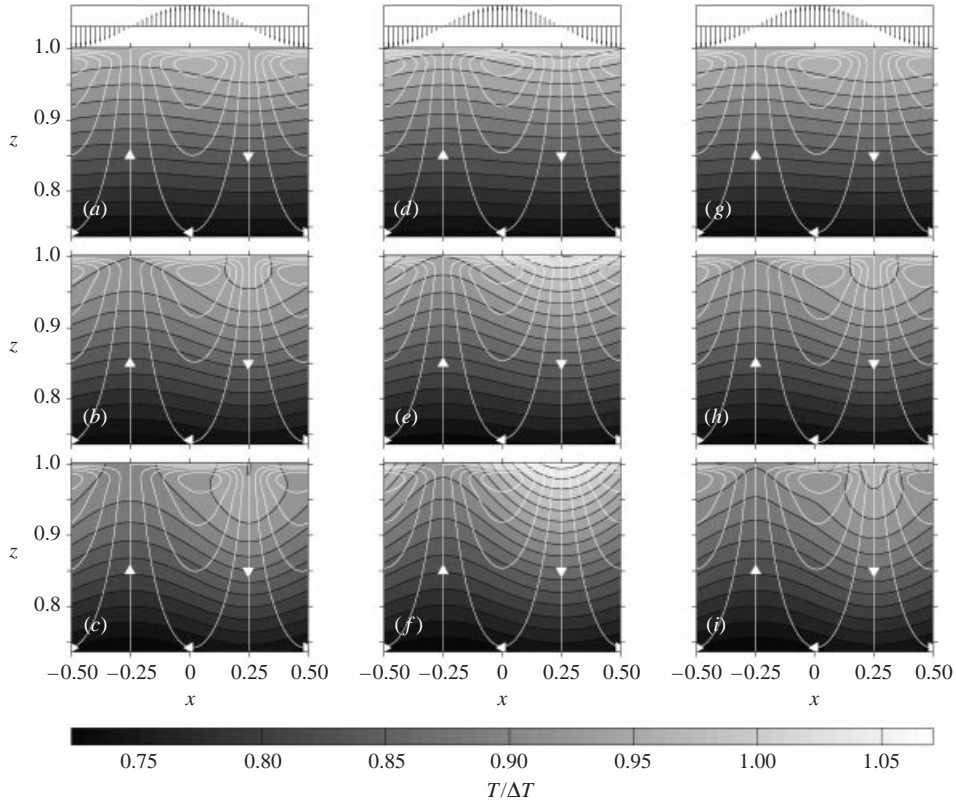


FIGURE 1. The numerical (*a–c*), classical linear SSU (*d–f*), and nonlinear SSU (*g–i*) solutions for the temperature and stream function (white contours) evaluated at $t = 0.10$ (upper row), $t = 0.31$ (middle row), and $t = 0.54$ (lower row). The nonlinear SSU solutions are valid to $O(\epsilon)$. A schematic of the wind-stress forcing is plotted at the top of each column.

numerical and classical SSU solutions for the stream function show the basic structure of intensified cross-wind flow in the upper Ekman layer, upwelling/downwelling at the maximum/minimum wind stress curl, and a weak interior secondary circulation that decays with depth. Notice that, unlike the classical SSU solution, the maximum and minimum values of the stream function of the numerical simulation are not located directly underneath the maximum and minimum wind stress, but are displaced towards the location of the minimum wind-stress curl. Like the stream function, the temperature field of both solutions shows similarities in the basic structure of warmer downwelled water to the right of $x = 0$ and cooler upwelled water to the left. However, the spatial structure and magnitudes of the two solutions are quite different. Within and beneath the Ekman layer, the spatial structure of the temperature field of the numerical model consists of steepened, vertical, or inverted isotherms near the surface, and a complex lateral structure with intensified horizontal gradients near $x = 0.25$, features that are absent from the classical SSU solution. Also notice that the temperature of the classical SSU solution exceeds the maximum temperature of the initial stratification even though there are no sources of heat; the numerical simulation does not develop this artefact. Like the stream function, the down-wind velocity of both solutions plotted in figure 2 is surface intensified and decays with depth as a consequence of the stratification. Another similarity between the stream

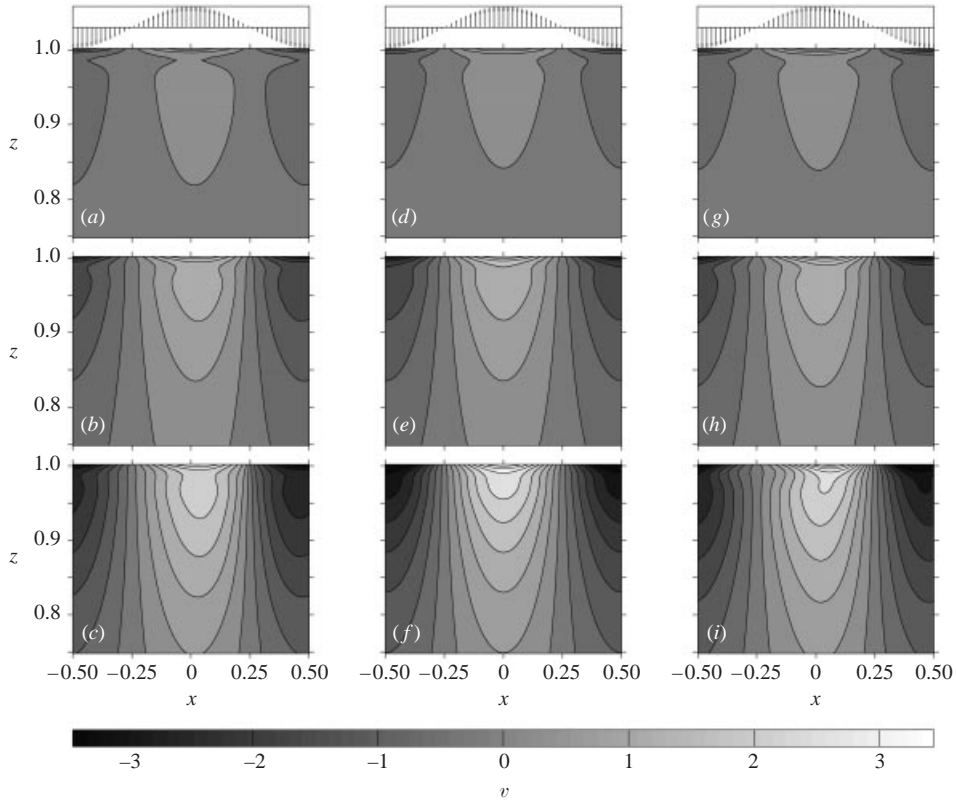


FIGURE 2. The numerical (*a–c*), classical linear SSU (*d–f*), and nonlinear SSU (*g–i*) solution for the down-wind velocity, non-dimensionalized by U , evaluated at $t = 0.10$ (upper row), $t = 0.31$ (middle row), and $t = 0.54$ (lower row). The nonlinear SSU solution is valid to $O(\epsilon)$. A schematic of the wind-stress forcing is plotted at the top of each column.

function and the down-wind velocity is that its maximum and minimum are shifted towards $x = 0.25$. The sinusoidal lateral structure of the classical SSU solution (3.13) cannot duplicate this feature. These failures of the classic SSU solution result from the disregard of horizontal advection of momentum/density and from the lack of a proper thermal boundary condition used in the theory. In this section, we will show that both of these deficiencies are significant, especially for the parameter range of this study (see table 1 as well as conditions (2.15) and (2.17)).

It is instructive to use the classical SSU solutions to estimate the strength of nonlinear advection of momentum in the Ekman layer (which is $E^{-1/2}$ times larger than advection of momentum by the interior secondary circulation). Using (3.3) and (3.13) the horizontal advection of y -momentum in the Ekman layer scales like $\epsilon u_e \partial v_i / \partial x \sim 2\pi\lambda\epsilon t$. Evaluating this estimate based on the parameters in table 1: for $t = 0.31$ $\epsilon u_e \partial v_i / \partial x \sim 0.25$, which is a fourth of the magnitude of the unit-scale Coriolis force. Hence, at this time, the neglect of the nonlinear advection of momentum in classical SSU theory should lead to significant differences between the classical SSU solutions and the fully nonlinear numerical solutions. Indeed, at this time the numerical solution for the velocity in the y -direction takes the form of a steepened sinusoid unlike the pure sinusoidal shape of v_i (figure 3*a*). The numerical solution of the temperature field likewise is not a simple sinusoid, taking an asymmetric form

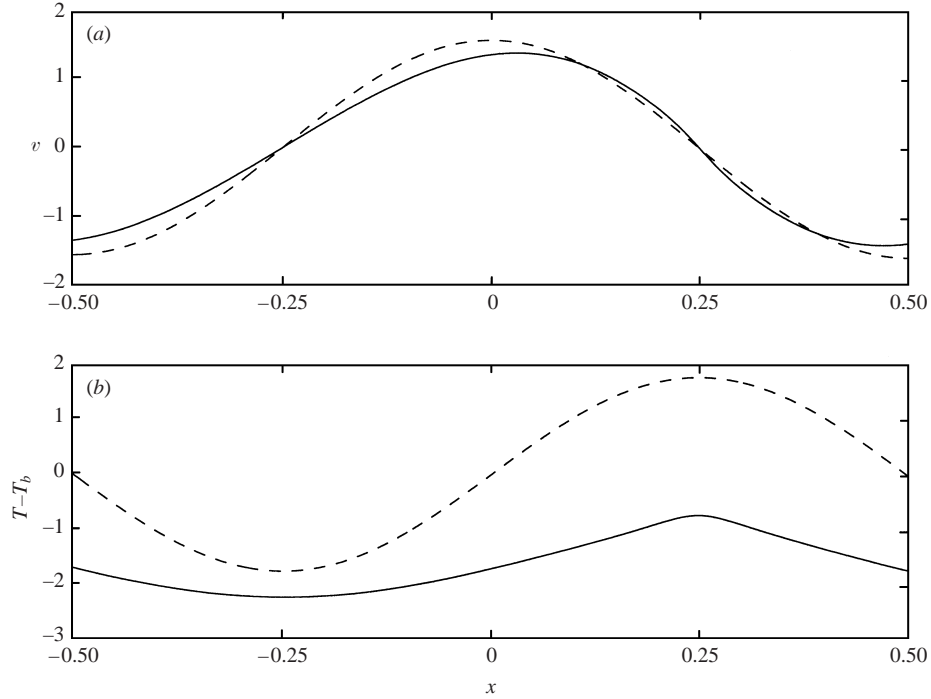


FIGURE 3. Lateral structure of the numerical (solid) and classical linear SSU (dashed) solutions for the down-wind velocity v (a) and the deviation of the temperature from the background uniform stratification $T - T_b$ (b) evaluated at $z = 0.982$ and $t = 0.31$. $T - T_b$ is non-dimensionalized by $\Delta T/\epsilon$.

about $x = 0$. The distortion of the lateral structure of the numerical solutions from that of the classical SSU solutions evident in figure 3 is attributable to horizontal advection of momentum and temperature, which we will show quantitatively in §4. Also notice that the horizontal average of the temperature field of the numerical model is non-zero, unlike the analytic solution. This non-zero lateral mean is attributable to the diffusion of the insulating boundary condition (2.11) into the fluid.

Even if no wind stress is applied to the stratified fluid, the temperature field will change with time near the horizontal boundaries since the background temperature field itself does not satisfy the insulating boundary conditions. Near these horizontal boundaries, thermal diffusion diminishes the stratification, generating growing thermal boundary layers of thickness $\delta_T = \sqrt{(\kappa/\sigma)\tau_h t} = HE^{1/4}\sqrt{t/(2\sigma)}$, which for $t \sim 1$ are $E^{-1/4}$ times thicker than the Ekman layers. These thermal boundary layers are clearly seen near the top and bottom of the domain in the vertical profile of the numerical solution of $T - T_b$ (figure 4). Notice that the magnitude of the deviation of the numerical model solution from the analytic solution is larger near $z = 1$ than $z = 0$. Since the secondary circulation is intensified near the surface, this asymmetry suggests that advection of temperature as well as diffusion plays a role in determining the structure of the temperature field in the thermal boundary layer.

From these comparisons between the classical SSU solutions and the numerical solutions we conclude that a proper theory of stratified spin-up must account for nonlinear advection of momentum and temperature and include a thermal boundary layer.

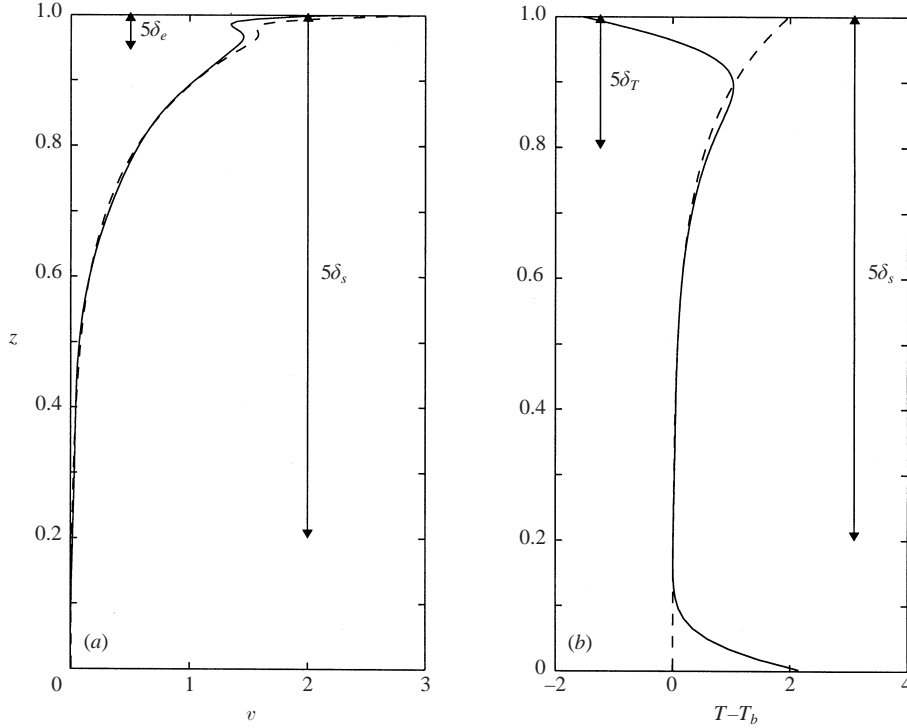


FIGURE 4. Vertical profiles of the numerical (solid) and classical SSU (dashed) solutions for the down-wind velocity evaluated at $x = 0$ (a), and $T - T_b$ evaluated at $x = 0.25$ (b). Both quantities are plotted at $t = 0.31$. Arrows indicate five times the thickness of the Ekman layer δ_e , the thermal boundary layer δ_T , and the Prandtl depth δ_s .

4. Nonlinear stratified spin-up theory

Similar to classical SSU theory, we split the dependent variables into interior and Ekman layer parts; we also include a thermal boundary layer. For example the down-wind velocity is decomposed as follows: $v = v_e + v_T + v_i$, where the subscript T denotes a thermal-boundary-layer variable. Although there are thermal boundary layers both at the top and bottom of the fluid layer, we will focus our analysis on the top layer where the secondary circulation and hence advection is much stronger. In this boundary layer, the variables are functions of the following stretched vertical coordinate: $\xi = (1 - z)/E^{1/4}$.

The theory uses a regular perturbation expansion in orders of the Rossby number. Because of (2.15), the Rossby number plays three roles in the expansions of the flow variables: it allows for a weakly nonlinear analysis, accounts for diffusion, and scales variables in the horizontal boundary layers according to the thickness of their respective boundary layers. Quantities in the Ekman layers are expanded in powers of $\epsilon^{1/2}$:

$$\psi_e = \sum_{n=0}^{\infty} \epsilon^{n/2} \psi_e^{(n)}, \quad v_e = \sum_{n=0}^{\infty} \epsilon^{n/2} v_e^{(n)}, \quad T_e = \sum_{n=0}^{\infty} \epsilon^{n/2} T_e^{(n)}. \quad (4.1)$$

Similar expansions are applied in the interior region

$$\psi_i = \sum_{n=0}^{\infty} \epsilon^{n/2} \psi_i^{(n)}, \quad v_i = \sum_{n=0}^{\infty} \epsilon^{n/2} v_i^{(n)}, \quad T_i = \sum_{n=0}^{\infty} \epsilon^{n/2} T_i^{(n)}, \quad (4.2)$$

while the thermal-boundary-layer variables are expanded as follows:

$$\psi_T = \epsilon \sum_{n=0}^{\infty} \epsilon^{n/2} \psi_T^{(n)}, \quad v_T = \epsilon^{1/2} \sum_{n=0}^{\infty} \epsilon^{n/2} v_T^{(n)}, \quad T_T = \epsilon^{-1/2} \sum_{n=0}^{\infty} \epsilon^{n/2} T_T^{(n)}. \quad (4.3)$$

The Ekman layer and interior stream functions are related to the cross-wind and vertical velocities by (3.4) and (3.5), whereas in the thermal boundary layer they are connected through

$$(u_T, w_T) = -E^{1/2}(E^{-1/4} \partial \psi_T / \partial \xi, \partial \psi_T / \partial x). \quad (4.4)$$

The logic behind the scaling of the thermal-boundary-layer variables will be explained in §§4.2 and 4.3.

The governing equations for the expanded variables are obtained by substituting (4.1), (4.2) and (4.3) into (2.6)–(2.9), using (2.15), noting that $\partial/\partial z = -(\gamma\epsilon)^{-1/2} \partial/\partial \xi = -(\gamma\epsilon)^{-1} \partial/\partial \eta$, and collecting terms of like order in Rossby number.

4.1. $O(1)$ solutions in the interior and Ekman layer

The $O(1)$ solutions in the interior and Ekman layer are identical to the classical SSU solutions described in §3.1. That is, $\psi_e^{(0)}$ is given by (3.3), $\psi_i^{(0)}$ by (3.12), $v_i^{(0)}$ by (3.13), and $T_i^{(0)}$ by (3.14). The temperature equation in the Ekman layer to $O(1)$ is $\partial^2 T_e^{(0)} / \partial \eta^2 = 0$, the solution of which is $T_e^{(0)} = a\eta + b$. For non-zero values of a and b , this solution does not meet the requirement that $T_e^{(0)} \rightarrow 0$ as $\eta \rightarrow \infty$. Thus, the only permissible solution for the temperature field to $O(1)$ in the Ekman layer is $T_e^{(0)} = 0$.

4.2. $O(\epsilon^{-1/2})$ and $O(1)$ temperature correction in the thermal boundary layer

The heat-flux boundary condition (2.11), rewritten in terms of the interior, thermal and Ekman layer temperature fields is

$$\frac{\partial T_T}{\partial \xi} = \epsilon^{-1/2} S \gamma^{1/2} - \epsilon^{-1/2} \gamma^{-1/2} \frac{\partial T_e}{\partial \eta} + \epsilon^{1/2} \gamma^{1/2} \frac{\partial T_i}{\partial z}. \quad (4.5)$$

Since the $O(1)$ temperature field in the Ekman layer is zero and therefore does not affect (4.5), an $O(\epsilon^{-1/2})$ correction to the temperature in the thermal boundary layer is needed to cancel the heat flux of the background temperature field at $z = 1$. The governing equation and boundary condition for $T_T^{(0)}$ is

$$\frac{\partial T_T^{(0)}}{\partial t} - \frac{1}{2} \frac{\partial^2 T_T^{(0)}}{\partial \xi^2} = 0, \quad (4.6)$$

$$\frac{\partial T_T^{(0)}}{\partial \xi} = S \gamma^{1/2} \quad \text{at} \quad \xi = 0. \quad (4.7)$$

Notice that the Prandtl number has not been explicitly included in (4.6) since it is equal to one. For the remainder of the paper the Prandtl number will be dropped from all forms of the temperature equation. The solution to the diffusion equation (4.6) subject to (4.7) is

$$T_T^{(0)} = -\sqrt{2t} S \gamma^{1/2} i \operatorname{erfc} \left(\frac{\xi}{\sqrt{2t}} \right), \quad (4.8)$$

where

$$i \operatorname{erfc}(\xi/\sqrt{2t}) = \int_{\xi/\sqrt{2t}}^{\infty} \operatorname{erfc}(s) ds$$

is the first repeated integral of the error function (Abramowitz & Stegun 1972).

The $O(1)$ temperature equation is

$$\frac{\partial T_T^{(1)}}{\partial t} - \frac{1}{2} \frac{\partial^2 T_T^{(1)}}{\partial \xi^2} = -\frac{1}{\gamma^{1/2}} \left(\frac{\partial \psi_i^{(0)}}{\partial x} \Big|_{z=1} \right) \frac{\partial T_T^{(0)}}{\partial \xi}, \quad (4.9)$$

which is a diffusion equation forced by the vertical advection of the $O(\epsilon^{-1/2})$ temperature field by the interior vertical velocity. The interior vertical velocity is approximated by its value at the surface. The variation of the interior vertical velocity across the relatively thin thermal boundary layer is at most $O(\epsilon^{1/2})$ and therefore is neglected at this level in the regular perturbation expansion.

The boundary condition on $T_T^{(1)}$ is determined from the $O(\epsilon^{1/2})$ correction to the temperature in the Ekman layer, which satisfies the equation $\partial^2 T_e^{(1)}/\partial \eta^2 = 0$. Since $T_e^{(1)} = 0$, it follows from (4.5) that

$$\frac{\partial T_T^{(1)}}{\partial \xi} = 0 \quad \text{at} \quad \xi = 0. \quad (4.10)$$

The solution to (4.9) subject to (4.10) is

$$T_T^{(1)} = -2\pi S \left[\xi \sqrt{2t} \operatorname{ierfc} \left(\frac{\xi}{\sqrt{2t}} \right) + 2t \operatorname{ierfc} \left(\frac{\xi}{\sqrt{2t}} \right) \right] \sin(2\pi x), \quad (4.11)$$

where

$$i^2 \operatorname{erfc}(\xi/\sqrt{2t}) = \int_{\xi/\sqrt{2t}}^{\infty} i \operatorname{erfc}(s) ds.$$

Including the $O(1)$ corrections to the temperature field in the thermal boundary layer greatly improves the solution relative to the classical SSU solution (i.e. compare figures 5(a) and the lower panel of figure 3(b) as well as figure 5(d) and the right panel of figure 4(b)). It improves the solution by capturing the non-zero negative lateral mean and the reduced peak-to-peak amplitude. To obtain a quantitative calculation of the amount by which the peak-to-peak amplitude is reduced, (4.11) was evaluated at $\xi = 0$ and added to the $O(1)$ interior temperature field: $T_T^{(1)}|_{\xi=0} + T_i^{(0)}|_{z=1} = \pi S t \sin(2\pi x)$. This calculation reveals that the temperature to $O(1)$ still grows secularly at the surface yet its amplitude is reduced by half. The reduction of amplitude of the $O(1)$ temperature field is a consequence of the diminished effective background stratification in the thermal boundary layer, i.e. $dT_b/dz - \Delta T/(HS\gamma^{1/2})\partial T_T^{(0)}/\partial \xi = (\Delta T/H) \operatorname{erf}(\xi/\sqrt{2t})$. As the effective background stratification diffuses away, the vertical advection of temperature must decrease, hence reducing advective warming and cooling. This result, which is ultimately attributable to the flux boundary condition on the temperature field, affects both the thermodynamics of the spin-up process and the dynamics of the down-wind velocity.

4.3. $O(\epsilon^{1/2})$ down-wind velocity corrections in the thermal boundary layer

The pressure in the thermal boundary layer p_T can be written in terms of the temperature via the hydrostatic relation

$$\frac{\partial p_T}{\partial \xi} = -(\gamma\epsilon)^{1/2}(\epsilon^{-1/2}T_T^{(0)} + T_T^{(1)} + \dots). \quad (4.12)$$

Using (4.12) to scale the pressure-gradient force in the x -direction, it is clear that the magnitude of this force is at most $O(\epsilon^{1/2})$, since $T_T^{(0)}$ is independent of x . In the thermal boundary layer, the scale of the acceleration, advection, and vertical diffusion

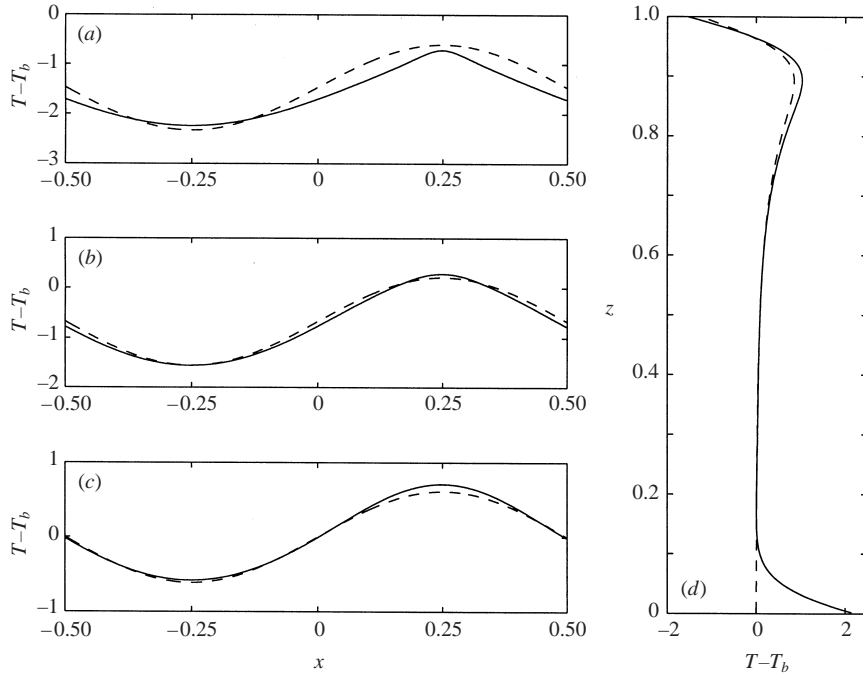


FIGURE 5. The nonlinear SSU solution for $T - T_b$ valid to $O(1)$ (dashed), i.e. $T^{(1)} \equiv \epsilon^{-1/2} T_T^{(0)} + T_T^{(1)} + T_i^{(0)}$, compared to the numerical solution (solid) for $t = 0.31$. The lateral structure of $T - T_b$ is plotted for (a) $z = 0.982$, (b) $z = 0.955$, and (c) $z = 0.815$. (d) Vertical profile of $T - T_b$ at $x = 0.25$.

terms in the x -momentum equation (2.6) is less than $O(\epsilon)$. Therefore, a geostrophic $O(\epsilon^{1/2})$ down-wind velocity is required to balance the pressure-gradient force in the thermal boundary layer. Once $T_T^{(1)}$ is known, this geostrophic flow can be calculated by vertically integrating the thermal-wind relation:

$$\frac{1}{\gamma^{1/2}} \frac{\partial v_T^{(0)}}{\partial \xi} = -\frac{\partial T_T^{(1)}}{\partial x}, \quad (4.13)$$

noting that $v_T^{(0)} \rightarrow 0$ as $\xi \rightarrow \infty$. Using (4.11), the thermal-wind relation (4.13) yields the following solution:

$$v_T^{(0)} = -8\pi^2 \gamma^{1/2} S \left[\xi t i^2 \operatorname{erfc} \left(\frac{\xi}{\sqrt{2t}} \right) + (2t)^{3/2} i^3 \operatorname{erfc} \left(\frac{\xi}{\sqrt{2t}} \right) \right] \cos(2\pi x), \quad (4.14)$$

where

$$i^3 \operatorname{erfc}(\xi/\sqrt{2t}) = \int_{\xi/\sqrt{2t}}^{\infty} i^2 \operatorname{erfc}(s) ds.$$

Throughout the thermal boundary layer, the amplitude of the down-wind velocity and its vertical shear is reduced relative to the classical SSU solution (compare figure 6d to figure 4a), drastically improving the vertical and lateral structure of the analytic solution. Hence, the thermal-boundary-layer temperature field is necessary for an accurate analytic solution of the down-wind velocity.

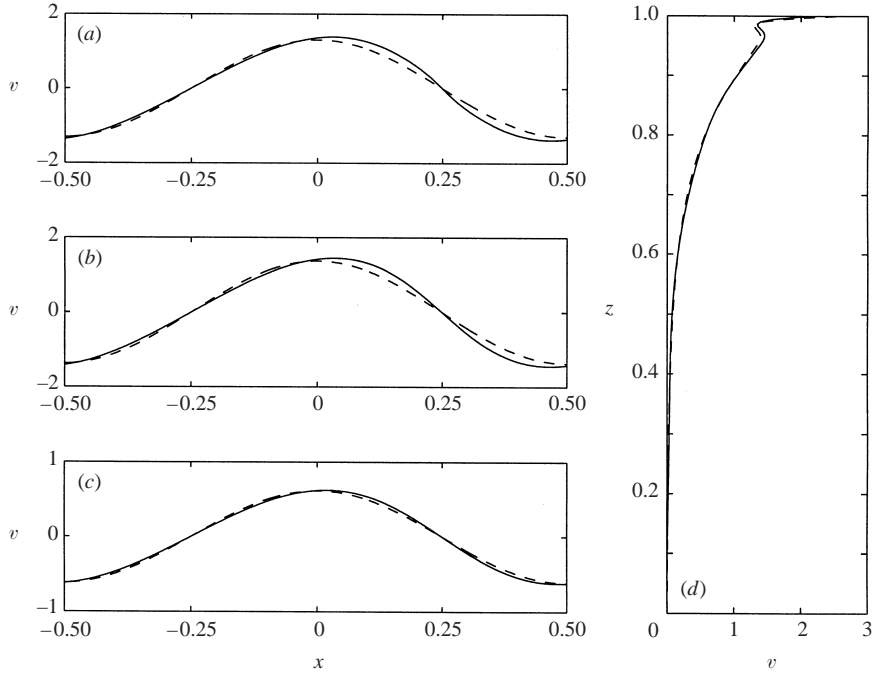


FIGURE 6. The nonlinear SSU solution for the down-wind velocity v valid to $O(\epsilon^{1/2})$ (dashed), i.e. $v^{(1)} \equiv v_e^{(0)} + v_i^{(0)} + \epsilon^{1/2}v_T^{(0)}$, compared to the numerical solution (solid) for $t = 0.31$. The lateral structure of v is plotted for (a) $z = 0.982$, (b) $z = 0.955$, and (c) $z = 0.815$. (d) Vertical profile of v at $x = 0$.

4.4. $O(\epsilon)$ solutions in the Ekman layer

The $O(\epsilon)$ velocities in the upper Ekman layer are forced by horizontal and vertical advection of the $O(1)$ momentum. We restrict our weakly nonlinear analysis to the upper Ekman layer and neglect nonlinear dynamics in the bottom Ekman layer. This is justifiable for Burger numbers of order-one, since the stratification considerably weakens the interior flow near the bottom. A nonlinear analysis of the bottom Ekman layer in a homogeneous fluid has most recently been done by Hart (2000), who analytically derived high-order corrections in Rossby number to the Ekman-pumping formula for a given interior geostrophic flow.

The second-order momentum equations in the top Ekman layer are

$$\frac{1}{2} \frac{\partial^2 u_e^{(2)}}{\partial \eta^2} + v_e^{(2)} = F_x \tag{4.15}$$

$$\frac{1}{2} \frac{\partial^2 v_e^{(2)}}{\partial \eta^2} - u_e^{(2)} = F_y, \tag{4.16}$$

where

$$F_x = u_e^{(0)} \frac{\partial u_e^{(0)}}{\partial x} + \frac{\partial}{\partial x} (\psi_e^{(0)} + \psi_i^{(0)}|_{z=1}) \frac{\partial u_e^{(0)}}{\partial \eta}, \tag{4.17}$$

$$F_y = u_e^{(0)} \left(\frac{\partial v_e^{(0)}}{\partial x} + \frac{\partial v_i^{(0)}}{\partial x} \Big|_{z=1} \right) + \frac{\partial}{\partial x} (\psi_e^{(0)} + \psi_i^{(0)}|_{z=1}) \frac{\partial v_e^{(0)}}{\partial \eta} \tag{4.18}$$

are the expressions for the divergence of the first-order x and y advective momentum fluxes within the top Ekman layer. Notice that they include terms involving interior quantities. These quantities are evaluated at $z = 1$ because their variation over the thin Ekman layer is negligible. By differentiating equation (4.15) twice with respect to the vertical coordinate, $v_e^{(2)}$ can be eliminated from equation (4.16) yielding the following equation for $u_e^{(2)}$:

$$\frac{\partial^4 u_e^{(2)}}{\partial \eta^4} + 4u_e^{(2)} = 2 \frac{\partial^2 F_x}{\partial \eta^2} - 4F_y. \quad (4.19)$$

The stress boundary conditions at $z = 1$ for the $O(\epsilon)$ velocities in the Ekman layer are

$$\frac{\partial v_e^{(2)}}{\partial \eta} = -2\tau_g \quad \text{at } z = 1, \quad (4.20)$$

$$\frac{\partial u_e^{(2)}}{\partial \eta} = 0 \quad \text{at } z = 1, \quad (4.21)$$

where we have introduced a ‘geostrophic stress’

$$\tau_g = -\frac{\gamma}{2} \left(\frac{\partial v_i^{(0)}}{\partial z} \Big|_{z=1} - \frac{1}{\gamma^{1/2}} \frac{\partial v_T^{(0)}}{\partial \xi} \Big|_{\xi=0} \right) \quad (4.22)$$

to correct for the geostrophic shear at the surface. Since the vertical structure of the terms on the right-hand side of (4.19) take the form of the real part of complex exponentials (i.e. $\text{Re}(e^{a\eta})$ where a is a complex number), an analytic expression for $u_e^{(2)}$ is easily obtained. Once this is done, $u_e^{(2)}$ can be integrated with respect to η to yield $\psi_e^{(2)}$:

$$\begin{aligned} \psi_e^{(2)} = & -\frac{1}{4} \{ \eta e^{-\eta} [\cos(\eta) + \sin(\eta)] + 4e^{-\eta} \cos(\eta) \} \cos(2\pi x) \frac{\partial v_i^{(0)}}{\partial x} \Big|_{z=1} \\ & -\pi \left[\frac{3}{10} e^{-2\eta} - \eta e^{-\eta} \cos(\eta) + \frac{8}{5} e^{-\eta} \sin(\eta) - \frac{4}{5} e^{-\eta} \cos(\eta) \right] \sin(4\pi x) \\ & -\frac{\gamma}{2} \left(\frac{\partial v_i^{(0)}}{\partial z} \Big|_{z=1} - \frac{1}{\gamma^{1/2}} \frac{\partial v_T^{(0)}}{\partial \xi} \Big|_{\xi=0} \right) e^{-\eta} \cos(\eta). \end{aligned} \quad (4.23)$$

By definition, the Ekman transport is equal to the Ekman-layer stream function evaluated at $\eta = 0$. Using (4.23), the dimensional Ekman transport including the $O(\epsilon)$ correction becomes

$$\begin{aligned} M = & \frac{\tau_o}{\rho f} (\psi_e^{(0)}|_{\eta=0} + \epsilon \psi_e^{(2)}|_{\eta=0} + \dots) \\ = & \frac{\tau_o}{\rho f} \cos(2\pi x) \left[1 - \underbrace{\epsilon \frac{\partial v_i^{(0)}}{\partial x} \Big|_{z=1}}_{\text{VORT}} + \underbrace{\epsilon \pi \sin(2\pi x)}_{\text{STEADY}} \right] + \underbrace{\left(\frac{\tau_o}{\rho f} \right) E^{1/2} \tau_g}_{\text{GSTRESS}} + \dots \end{aligned} \quad (4.24)$$

Comparing this result to that of Stern (1965) and Niiler (1969), (1.1), it is clear that the first two terms in (4.24) are identical to the first two terms of an expansion in ζ/f of M_{nl} if the vertical vorticity used in (1.1) is calculated from the interior down-wind flow. The STEADY term in (4.24) arises from horizontal and vertical advection of the

momentum of the flow in the Ekman layer and is constant in time. The GSTRESS term in (4.24) illustrates the way in which the flow in the Ekman layer responds to the ‘geostrophic stress’ in a completely analogous fashion as to the wind stress.

Notice that the Ekman transport is enhanced (reduced) where the interior vertical vorticity is anticyclonic (cyclonic). To gain physical insight into this feature of the solution, it is beneficial to look at the equation governing the x -component, $\omega_x = \partial v_e / \partial \eta$, of the relative vorticity in the Ekman layer. To single out the physics involving the interior vorticity term in (4.24), only the term involving the advection of v_i will be considered. Also, since we are interested in the dynamics in the thin Ekman layer, the vertical variation of the vertical vorticity as well as horizontal diffusion will be neglected. The approximate equation for ω_x is

$$\left(1 + \epsilon \frac{\partial v_i}{\partial x} \Big|_{z=1}\right) \frac{\partial u_e}{\partial \eta} = \frac{1}{2} \frac{\partial^2 \omega_x}{\partial \eta^2}. \quad (4.25)$$

The physics behind this equation is best described in terms of tilting of vorticity. By including the nonlinear term in the equation, the tilting of absolute rather than planetary vorticity replenishes frictional twisting, which dissipates ω_x . Because of this, the shear in the Ekman layer must be enhanced in regions of anticyclonic vorticity so that the tilting of the diminished absolute vorticity can balance the dissipation.

4.5. $O(\epsilon)$ stream function in the thermal boundary layer

The $O(\epsilon)$ stream function is a residual circulation that allows $v_T^{(0)}$ to satisfy both the thermal-wind relation (4.13) and the y -momentum equation in the thermal boundary layer:

$$\frac{\partial v_T^{(0)}}{\partial t} - \frac{1}{2} \frac{\partial^2 v_T^{(0)}}{\partial \xi^2} = \frac{1}{\gamma^{1/2}} \frac{\partial \psi_T^{(0)}}{\partial \xi}. \quad (4.26)$$

A single equation for $\psi_T^{(0)}$ can be obtained using the thermal-wind relation (4.13) and the equation for the $O(1)$ thermal-boundary-layer temperature field (4.9):

$$\frac{\partial^2 \psi_T^{(0)}}{\partial \xi^2} - \gamma^{1/2} \left(\frac{\partial^2 \psi_i^{(0)}}{\partial x^2} \Big|_{z=1} \right) \frac{\partial T_T^{(0)}}{\partial \xi} = 0. \quad (4.27)$$

Notice that this equation for the thermal-boundary-layer stream function resembles the equation governing $\psi_i^{(0)}$ (3.9). This similarity sheds light on the physical interpretation of the $O(\epsilon)$ thermal-boundary-layer stream function. In physical terms, both (4.27) and (3.9) state that laterally varying vertical advection of density must be compensated by vertically sheared Coriolis acceleration so that the spun-up down-wind flow remains in a thermal-wind balance. Since the stratification and hence the vertical advection of density is diminished in the thermal boundary layer as a consequence of the insulating boundary condition, the Coriolis acceleration and thus the cross-wind flow must be reduced in this boundary layer as well. The solution to (4.27), noting that $\psi_T^{(0)} \rightarrow 0$ as $\xi \rightarrow \infty$, is

$$\psi_T^{(0)} = 8\pi^2 S \gamma t^2 \operatorname{erfc} \left(\frac{\xi}{\sqrt{2t}} \right) \cos(2\pi x), \quad (4.28)$$

which yields a cross-wind flow everywhere to the right of the wind stress and generates a Coriolis acceleration opposite to that of the interior $O(1)$ secondary circulation. This weakening of the Coriolis force by $\psi_T^{(0)}$ is responsible for the reduced amplitude

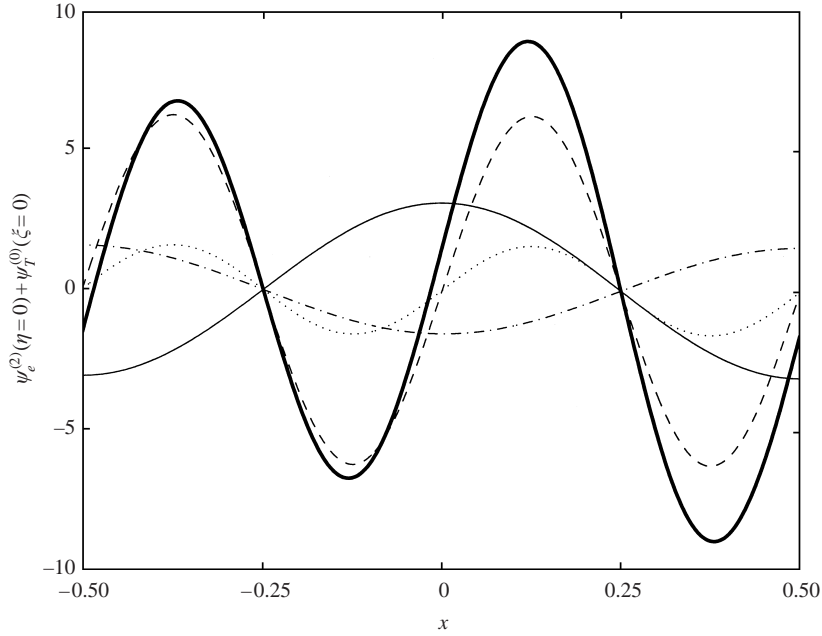


FIGURE 7. The sum of the $O(\epsilon)$ cross-wind transport in the Ekman and thermal boundary layers (thick solid) and its constituents evaluated at $t = 0.31$. The constituents include the STEADY (dotted), VORT (dashed), and GSTRESS (dash-dotted) terms, see (4.24), as well as the thermal-boundary-layer transport (thin solid).

of the $O(\epsilon^{1/2})$ down-wind velocity relative to the classical SSU solution illustrated in figure 6.

4.6. $O(\epsilon)$ correction to the stream function in the interior

To satisfy the no-normal-flow boundary condition at the surface, the interior vertical velocity must be equal and opposite to the suction/pumping of fluid out of both the Ekman and thermal boundary layers. This requirement sets the boundary condition for the $O(\epsilon)$ correction to the interior stream function, $\psi_i^{(2)}$, at the surface:

$$\psi_i^{(2)} = -\psi_e^{(2)} - \psi_T^{(0)} \quad \text{at } z = 1. \quad (4.29)$$

Using the definitions for the Ekman transport and the total cross-wind transport of fluid across the thermal boundary layer,

$$M_T \equiv \int_0^\infty (-\partial\psi_T/\partial\xi) d\xi = \psi_T|_{\xi=0},$$

it is clear that $\psi_i^{(2)}$ is equal to the negative of the sum of the cross-wind transport in the Ekman and thermal boundary layers. The sum of these transports primarily follows the VORT term of (4.24), yet is distorted by both the Ekman transport associated with the ‘geostrophic stress’ and the thermal-boundary-layer transport (figure 7). Notice that while the Ekman pumping/suction associated with the ‘geostrophic stress’ is counter to the Ekman pumping/suction of the $O(1)$ solution (3.3), the pumping/suction associated with the thermal-boundary-layer transport augments that of the $O(1)$ solution. Since the pumping/suction associated with the thermal-boundary-layer transport is larger in magnitude than that of the ‘geostrophic stress’ (i.e. compare

the amplitudes of the thin-solid and dash-dotted curves in the figure), the net effect of these transports (which arise from diffusive rather than nonlinear dynamics and hence would be retained in a purely linear analysis) is to accelerate the spin-up process in the interior of the fluid. This result is a consequence of the flux boundary condition on the temperature field and thus depends on the value of the heat flux at the surface. In fact, it can be shown that if heat is inputted to the fluid at the surface, depending on the strength of the heat flux, the cross-wind transport in the thermal boundary layer will be reduced or even reversed from its value obtained using the insulating boundary condition (2.11). This illustrates the importance of the heat-flux boundary condition on the mechanics of SSU and on the secondary circulation in the interior.

The second-order correction to the stream function in the interior is governed by the following equation:

$$\frac{\partial^2 \psi_i^{(2)}}{\partial z^2} + S \frac{\partial^2 \psi_i^{(2)}}{\partial x^2} = 2J \left(v_i^{(0)}, \frac{\partial \psi_i^{(0)}}{\partial z} \right), \quad (4.30)$$

where J is the Jacobian operator, and is subject to (4.29) and

$$\frac{\partial \psi_i^{(2)}}{\partial t} = \frac{1}{2} \frac{\partial \psi_i^{(2)}}{\partial z} \quad \text{at } z = 0. \quad (4.31)$$

Equation (4.30) can be solved by splitting $\psi_i^{(2)}$ into a particular ψ_p solution and a homogeneous solution ψ_h . The particular solution to (4.30) is

$$\psi_p = \frac{\pi\lambda}{\sinh(2\lambda)} \left\{ \frac{(1 - e^{-\beta t})^2}{\beta} - e^{-\beta t} \left[t - \frac{(1 - e^{-\beta t})}{\beta} \right] \right\} \left(1 + \frac{\lambda}{2} z e^{-2\lambda z} \right) \sin(4\pi x). \quad (4.32)$$

This function is maximum at $z = 1/(2\lambda)$ where for $S = 1$, $t = 0.31$ and $x = \pi/8$ it is equal to $\psi_p = 1.2 \times 10^{-5}$. The magnitude of the homogeneous solution is set by the sum of the $O(\epsilon)$ cross-wind transport in the Ekman and thermal boundary layers. At $t = 0.31$ the maximum magnitude of $\psi_e^{(2)} + \psi_T^{(0)}$ at the surface is over five orders of magnitude greater than the maximum of the particular solution (figure 7). Thus the particular solution is a minute correction to $\psi_i^{(2)}$ and it will be neglected. If we write $\psi_e^{(2)}|_{\eta=0} = \Psi_1^e(t) \cos(2\pi x) + \Psi_2^e(t) \sin(4\pi x)$ and $\psi_T^{(0)}|_{\xi=0} = \Psi_1^T(t) \cos(2\pi x)$, then the homogeneous solution (and hence approximate total solution) of (4.30) is readily obtained:

$$\psi_i^{(2)} \simeq \sum_{n=1}^2 \left[D_n(t) \frac{\sinh(\lambda_n z)}{\sinh(\lambda_n)} + E_n(t) \frac{\cosh(\lambda_n z)}{\cosh(\lambda_n)} \right] \begin{cases} \cos(2\pi x) & (n = 1) \\ \sin(4\pi x) & (n = 2) \end{cases}, \quad (4.33)$$

with

$$E_n(t) = -\beta_n e^{-\beta_n t} \int_0^t e^{\beta_n s} [\Psi_n^e(s) + \Psi_n^T(s)] ds,$$

$$D_n(t) = -[\Psi_n^e(t) + \Psi_n^T(t)] - E_n(t)$$

and $\lambda_n = 2\pi n \sqrt{S}$ and $\beta_n = \lambda_n \coth(\lambda_n)/2$. We now have all the components of the stream function valid to $O(\epsilon)$: $\psi^{(2)} \equiv \psi_e^{(2)} + \psi_i^{(2)} + \epsilon(\psi_e^{(2)} + \psi_i^{(2)} + \psi_T^{(0)})$. The stream function valid to $O(\epsilon)$ is shown in figure 8 along with the result of the numerical experiment; it is also contoured in figure 1(g-i). The numerical model's output shows a strong signal at the inertial frequency. To compare this numerical solution to the analytical prediction, which does not include inertial oscillations, we filtered the numerical model's output using a Butterworth low-pass filter with a cut-off frequency

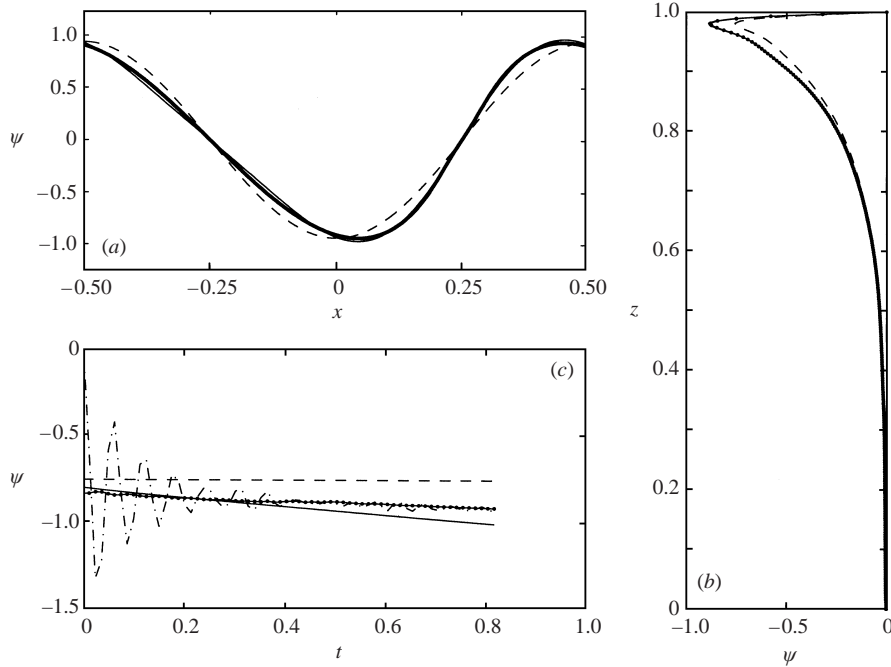


FIGURE 8. Nonlinear SSU solution for stream function ψ including the $O(\epsilon)$ correction, i.e. $\psi^{(2)} \equiv \psi_e^{(0)} + \psi_i^{(0)} + \epsilon(\psi_e^{(2)} + \psi_i^{(2)} + \psi_T^{(0)})$. (a) Lateral structure of analytical (solid) and temporally filtered numerical solution (dots) of ψ at $z = 0.98$ and $t = 0.31$; (b) vertical structure of ψ at the same time but at $x = 0.1$. (c) The time dependence of the unfiltered (dash-dotted) and filtered (dots) numerical solutions as well as that of the analytical theory (solid) at $x = 0.1$ and $z = 0.98$. Contrast this to classical linear SSU theory, depicted by the dashed curves in all three panels, which predicts a purely sinusoidal lateral structure and a time independent circulation.

of $0.75f$. $\psi^{(2)}$ and the filtered numerical solution evaluated at $x = 0.1$ and $z = 0.98$ deviate from the classical SSU solution, both being larger in magnitude and having a time dependence (figure 8c). The offset of $\psi^{(2)}$ from the classical SSU solution is evidently due to the time-independent part of the solution for $\psi_e^{(2)}$, i.e. the terms between the square brackets in (4.23). As alluded to previously, these terms arise from horizontal and vertical advection of the momentum of the flow in the Ekman layer. The linear decrease (yet increase in magnitude) of $\psi^{(2)}$ with time predicted by the theory agrees well with the trend of the numerical model for $t < 0.4$. This trend primarily results from the secular decrease in time of the vertical component of the interior first-order relative vorticity $\partial v_i^{(0)}/\partial x$ occurring between $x = 0$ and $x = 0.5$, which reduces the absolute vorticity, and thus enhances the Ekman transport. The effect of nonlinear dynamics is also seen in the lateral variation of the stream function at $t = 0.31$ (figure 8a). The most striking feature of the solution is its asymmetry about $x = 0$, having sharper gradients on the side of the peak in which $\partial v_i^{(0)}/\partial x$ is less than zero (i.e. $0 < x < 0.5$). From the relation between the vertical velocity and the stream function, (3.4), (3.5) and (4.4), it is evident that this asymmetry leads to narrow regions of enhanced downwelling in these anticyclonic zones and wider regions of reduced upwelling in cyclonic zones. The difference between $\psi^{(2)}$ and the numerical solution is barely distinguishable, from their vertical profiles plotted in figure 8(b). Above $z = 0.7$, both of these solutions are larger in magnitude than the classical SSU solution. This indicates that the modification of the secondary circulation by

nonlinearities in the Ekman layer does not penetrate throughout the full depth of the fluid, but is confined to the surface within a Prandtl depth based on the second harmonic of the forcing, i.e. $\delta_s^{(2)} = H/\lambda_2$.

4.7. $O(\epsilon^{1/2})$ and $O(\epsilon)$ temperature corrections

In the previous two sections we have shown how nonlinear advection of momentum in the Ekman layer modifies the secondary circulation. We now calculate the response of the fluid to horizontal advection of temperature by the Ekman flow. Horizontal advection of temperature by the Ekman flow directly affects the $O(\epsilon)$ Ekman-layer temperature field $T_e^{(2)}$, i.e.

$$\frac{\partial^2 T_e^{(2)}}{\partial \eta^2} = -2 \frac{\partial \psi_e^{(0)}}{\partial \eta} \left(\frac{\partial T_i^{(0)}}{\partial x} \Big|_{z=1} + \frac{\partial T_T^{(1)}}{\partial x} \Big|_{\xi=0} \right), \quad (4.34)$$

yet also, through the flux boundary condition on the temperature field

$$\frac{\partial T_T^{(2)}}{\partial \xi} = -\gamma^{-1/2} \frac{\partial T_e^{(2)}}{\partial \eta} + \gamma^{1/2} \frac{\partial T_i^{(0)}}{\partial z} \quad \text{at} \quad \xi = 0, \quad (4.35)$$

modulates the $O(\epsilon^{1/2})$ temperature field in the thermal boundary layer. By integrating the $O(\epsilon)$ Ekman-layer temperature equation with respect to η , the Ekman-layer temperature field can be eliminated from (4.35) yielding the boundary condition for $T_T^{(2)}$:

$$\frac{\partial T_T^{(2)}}{\partial \xi} = \underbrace{\frac{2}{\gamma^{1/2}} \psi_e^{(0)} \Big|_{\eta=0} \left(\frac{\partial T_i^{(0)}}{\partial x} \Big|_{z=1} + \frac{\partial T_T^{(1)}}{\partial x} \Big|_{\xi=0} \right)}_{\text{QADV}} + \gamma^{1/2} \frac{\partial T_i^{(0)}}{\partial z}. \quad (4.36)$$

This boundary condition has an elegant physical meaning. As dictated by equation (4.34), diffusion is strong enough in the Ekman layer to exactly balance horizontal advection of temperature by Ekman flow. For the stratified spin-up problem, relatively cool upwelled water is advected towards the warmer downwelled water by the Ekman flux. This would cool the Ekman layer if it were not balanced by diffusion. Diffusion extracts heat from the thermal boundary layer to counteract this cooling tendency. Thus QADV represents the heat flux leaving the thermal boundary layer to warm the advectively cooled Ekman layer. The last term in (4.36) is needed to correct for the non-zero heat flux of the interior $O(1)$ temperature field at $z = 1$.

The $O(\epsilon^{1/2})$ temperature equation in the thermal boundary layer is

$$\frac{\partial T_T^{(2)}}{\partial t} - \frac{1}{2} \frac{\partial^2 T_T^{(2)}}{\partial \xi^2} = -\frac{1}{\gamma^{1/2}} \left(\frac{\partial \psi_i^{(0)}}{\partial x} \Big|_{z=1} \right) \frac{\partial T_T^{(1)}}{\partial \xi} + \xi \left(\frac{\partial^2 \psi_i^{(0)}}{\partial x \partial z} \Big|_{z=1} \right) \frac{\partial T_T^{(0)}}{\partial \xi}. \quad (4.37)$$

It is evident that the forcing on the right-hand side of (4.37) accounts for the vertical advection of $T_T^{(1)}$ as well as the $O(\epsilon^{1/2})$ variation of the vertical structure of the interior vertical velocity across the relatively thin thermal boundary layer. To solve (4.37) subject to (4.36), $T_T^{(2)}$ was split into two parts: $T_T^{(2)} = T_{pa} + T_{bc}$, where T_{pa} solves equation (4.37) subject to the no-flux boundary condition: $\partial T_{pa} / \partial \xi = 0$, and T_{bc} solves the homogeneous form of equation (4.37) and satisfies (4.36); also, the

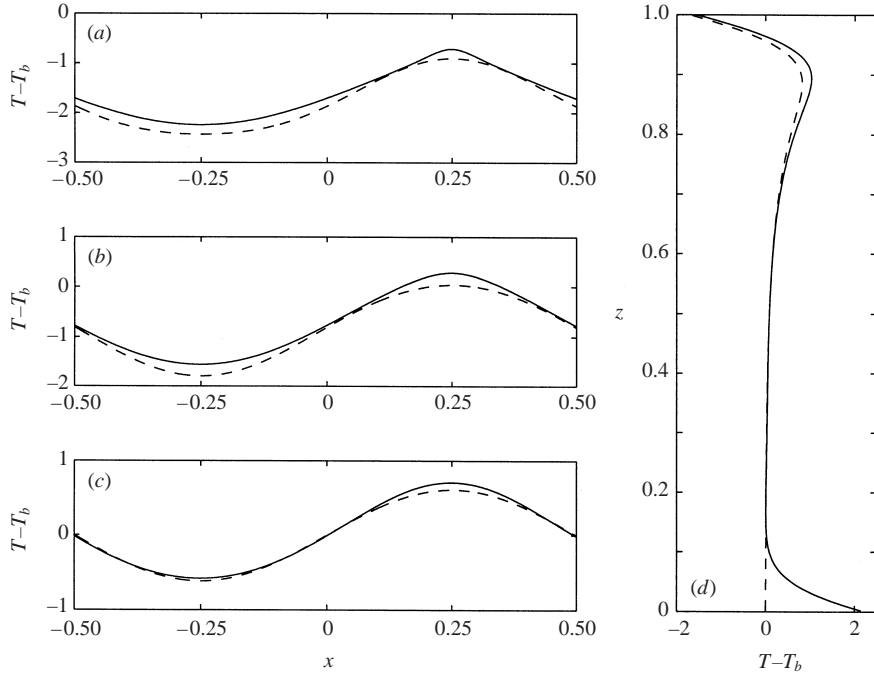


FIGURE 9. Same as figure 5 but for the nonlinear SSU solution for $T - T_b$ valid to $O(\epsilon^{1/2})$, i.e. $T^{(2)} \equiv \epsilon^{-1/2} T_T^{(0)} + T_T^{(1)} + T_i^{(0)} + \epsilon^{1/2} T_T^{(2)}$. At this order, horizontal advection of temperature in the Ekman layer affects the solution.

simplification $\tanh(\lambda) = 0.999993 \approx 1$ was utilized. The two parts of the solutions are

$$T_{bc} = -(2t)^{3/2} i^3 \operatorname{erfc} \left(\frac{\xi}{\sqrt{2t}} \right) \left\{ \underbrace{\frac{(2\pi)^2 S}{\gamma^{1/2}} [1 + \cos(4\pi x)] + 4\pi \lambda \gamma^{1/2} S \sin(2\pi x)}_{\text{HADVT}} \right\}, \quad (4.38)$$

$$T_{pa} = H(\xi, t) \left\{ -\frac{\pi^2 S}{\gamma^{1/2}} [1 - \cos(4\pi x)] + \pi \lambda \gamma^{1/2} S \sin(2\pi x) \right\}, \quad (4.39)$$

where

$$H(\xi, t) = \left[\sqrt{2t} \xi^2 i \operatorname{erfc} \left(\frac{\xi}{\sqrt{2t}} \right) + 2t \xi i^2 \operatorname{erfc} \left(\frac{\xi}{\sqrt{2t}} \right) + (2t)^{3/2} i^3 \operatorname{erfc} \left(\frac{\xi}{\sqrt{2t}} \right) \right].$$

By solving for $T_T^{(2)}$ in this way, the part of the temperature field attributable to the horizontal advection of temperature by the Ekman flow has been isolated, and is denoted by the HADVT term in (4.38).

Within the Ekman layer, the location of the maximum and minimum lateral temperature gradient for the temperature field including this $O(\epsilon^{1/2})$ correction has shifted towards the location of the minimum wind-stress curl (figure 9a). The temperature field of the analytical solution tends to be cooler than the numerical solution near $x = 0.25$ and -0.25 . This is because, up to this order of the expansion for the temperature, the unequal strength of upwelling and downwelling that results from the nonlinear modification of the Ekman transport is not incorporated into the dynamics of the temperature field. Because downwelling is enhanced near $x = 0.25$ and

upwelling is reduced near $x = -0.25$ the temperature should increase at both of these locations. We will now show that by adding the $O(\epsilon)$ correction to the temperature field in the interior and the thermal boundary layer, this feature of the solution is obtained.

The solution for the $O(\epsilon)$ correction to the interior temperature is obtained by integrating the interior $O(\epsilon)$ temperature equation:

$$\frac{\partial T_i^{(2)}}{\partial t} = -J(\psi_i^{(0)}, T_i^{(0)}) + S \frac{\partial \psi_i^{(2)}}{\partial x} + \frac{\gamma}{2} \frac{\partial^2 T_i^{(0)}}{\partial z^2}. \tag{4.40}$$

The first term on the right-hand side of (4.40) is the convergence of the interior advective heat flux. At the surface, where the components of this term are strongest, these components are

$$-\frac{\partial \psi_i^{(0)}}{\partial z} \frac{\partial T_i^{(0)}}{\partial x} = -\frac{\lambda^3 t}{2} (1 + \cos(4\pi x)), \tag{4.41}$$

$$\frac{\partial \psi_i^{(0)}}{\partial x} \frac{\partial T_i^{(0)}}{\partial z} = -\frac{\lambda^3 t}{2} (1 - \cos(4\pi x)), \tag{4.42}$$

where the simplification $\tanh(\lambda) = 0.999993 \approx 1$ has been used. The second term on the right-hand side of (4.40) represents the vertical advection of the background temperature field by the $O(\epsilon)$ interior vertical velocity. As stated previously, the largest term in the correction to the Ekman-layer stream function (4.23) is the term involving the interior vertical vorticity. Knowing this, and that at the surface $\psi_i^{(2)} = -\psi_e^{(2)} - \psi_T^{(0)}$, the second term on the right-hand side (4.40) predominantly has the form

$$S \frac{\partial \psi_i^{(2)}}{\partial x} = -\lambda^3 t \cos(4\pi x) + \dots \tag{4.43}$$

The effect of this term is to warm the fluid at $x = 0.25$ and -0.25 and thus will improve the analytic solution of the temperature field. Notice that both components of the interior advection terms (4.41) and (4.42) are comparable in magnitude to (4.43) but that the sum of (4.41) and (4.42) has no lateral dependence, unlike (4.43). Hence, interior advection does not affect the horizontal thermal gradient nor the geostrophic down-wind flow. To see this more explicitly, consider the $O(\epsilon)$ equation for the interior vertical vorticity, $\zeta_i^{(2)} = \partial v_i^{(2)} / \partial x$:

$$\frac{\partial \zeta_i^{(2)}}{\partial t} = \underbrace{-\frac{\partial \psi_i^{(0)}}{\partial z} \frac{\partial \zeta_i^{(0)}}{\partial x}}_{\text{HADV}} + \underbrace{\frac{\partial \psi_i^{(0)}}{\partial x} \frac{\partial \zeta_i^{(0)}}{\partial z}}_{\text{VADV}} - \underbrace{\frac{\partial^2 \psi_i^{(0)}}{\partial x \partial z} \zeta_i^{(0)}}_{\text{STR}\zeta} + \underbrace{\frac{\partial^2 \psi_i^{(0)}}{\partial x^2} \frac{\partial v_i^{(0)}}{\partial z}}_{\text{TILT}} - \frac{\partial^2 \psi_i^{(2)}}{\partial x \partial z} + \frac{\gamma}{2} \frac{\partial^2 \zeta_i^{(0)}}{\partial z^2}, \tag{4.44}$$

where $\zeta_i^{(0)} = \partial v_i^{(0)} / \partial x$. By evaluating the nonlinear terms in (4.44) at the surface, where they are largest in magnitude, and using the simplification $\tanh(\lambda) = 0.999993 \approx 1$, it can be shown that horizontal advection of $O(1)$ interior vertical vorticity, HADV, exactly cancels tilting of the $O(1)$ interior x -component of the vorticity to the vertical, TILT, while vertical advection, VADV, negates the stretching of $O(1)$ interior vertical vorticity, STR ζ . We can therefore conclude that the dynamics in the interior of the fluid, for SSU in which the Burger number is order-one, are predominantly linear, driven by Ekman pumping modified by nonlinearity in the Ekman layer.

The equation governing the $O(\epsilon)$ correction to the thermal boundary temperature

is much more complex than (4.40):

$$\begin{aligned} \frac{\partial T_T^{(3)}}{\partial t} - \frac{1}{2} \frac{\partial^2 T_T^{(3)}}{\partial \xi^2} = & -\frac{1}{\gamma^{1/2}} \left(\frac{\partial \psi_i^{(0)}}{\partial x} \Big|_{z=1} \right) \frac{\partial T_T^{(2)}}{\partial \xi} - \frac{1}{\gamma^{1/2}} \left(\frac{\partial \psi_i^{(2)}}{\partial x} \Big|_{z=1} \right) \frac{\partial T_T^{(0)}}{\partial \xi} \\ & + \frac{\partial \psi_T^{(0)}}{\partial x} \left(S - \frac{1}{\gamma^{1/2}} \frac{\partial T_T^{(0)}}{\partial \xi} \right) - \frac{1}{\gamma^{1/2}} \left(\frac{\partial \psi_i^{(0)}}{\partial z} \Big|_{z=1} \right) \frac{\partial T_T^{(1)}}{\partial x} \\ & + \xi \left(\frac{\partial^2 \psi_i^{(0)}}{\partial x \partial z} \Big|_{z=1} \right) \frac{\partial T_T^{(1)}}{\partial \xi} - \xi^2 \frac{\gamma^{1/2}}{2} \left(\frac{\partial^3 \psi_i^{(0)}}{\partial x \partial z^2} \Big|_{z=1} \right) \frac{\partial T_T^{(0)}}{\partial \xi}. \end{aligned} \quad (4.45)$$

At this order the insulating boundary condition takes the form

$$\frac{\partial T_T^{(3)}}{\partial \xi} = -\gamma^{-1/2} \frac{\partial T_e^{(3)}}{\partial \eta} \quad \text{at } \xi = 0, \quad (4.46)$$

which requires knowledge of the $O(\epsilon^{3/2})$ correction to the temperature field in the Ekman layer. $T_e^{(3)}$ is governed by the following equation:

$$\frac{\partial^2 T_e^{(3)}}{\partial \eta^2} = -2 \frac{\partial \psi_e^{(0)}}{\partial \eta} \left(\frac{\partial T_T^{(2)}}{\partial x} \Big|_{\xi=0} \right) + 2\gamma\eta \frac{\partial \psi_e^{(0)}}{\partial x} \frac{\partial^2 T_T^{(0)}}{\partial \xi^2} \Big|_{\xi=0}, \quad (4.47)$$

in which vertical diffusion of temperature balances horizontal and vertical advection of the thermal-boundary-layer temperature by the Ekman flow. On account of the no-flux boundary condition on the temperature, which makes the stratification weak in the Ekman layer, only the $O(\epsilon^{1/2})$ vertical variation of $T_T^{(0)}$ across the Ekman layer, i.e. $\partial T_T^{(0)}/\partial \xi = (\partial T_T^{(0)}/\partial \xi)|_{\xi=0} + \gamma^{1/2} \epsilon^{1/2} \eta (\partial^2 T_T^{(0)}/\partial \xi^2)|_{\xi=0} + \dots$, plays a role in the vertical advection term of (4.47). Vertical integration of (4.47) yields the boundary condition for $T_T^{(3)}$:

$$\frac{\partial T_T^{(3)}}{\partial \xi} = \frac{2}{\gamma^{1/2}} \psi_e^{(0)} \Big|_{\eta=0} \left(\frac{\partial T_T^{(2)}}{\partial x} \Big|_{\xi=0} \right). \quad (4.48)$$

Equation (4.45) subject to (4.48) was solved numerically.

The third component of the $O(\epsilon)$ correction to the temperature is $T_e^{(2)}$:

$$T_e^{(2)} = \pi^2 S t e^{-\eta} [\cos(\eta) - \sin(\eta)] [1 + \cos(4\pi x)]. \quad (4.49)$$

We now have all of the components of the temperature field valid to $O(\epsilon)$: $T^{(3)} \equiv \epsilon^{-1/2} T_T^{(0)} + T_T^{(1)} + T_i^{(0)} + \epsilon^{1/2} T_T^{(2)} + \epsilon (T_T^{(3)} + T_i^{(2)} + T_e^{(2)})$. Plotted in figure 10 is $T^{(3)}$ evaluated at $t = 0.31$. Comparing $T^{(3)}$ to $T^{(2)}$, it is evident that by accounting for the asymmetry in strength of downwelling versus upwelling in the thermodynamics, the analytical solution for the temperature field is greatly improved. $T^{(3)}$ plus the background temperature field is contoured in figure 1(g-i). The figure illustrates how the analytic solution is able to capture the extreme features of temperature inversions and vertical isotherms found in the numerical solution (figure 1a-c).

4.8. $O(\epsilon)$ corrections to the down-wind velocity

We now have all that is needed to calculate the $O(\epsilon)$ corrections to the down-wind velocity in the Ekman layer, thermal boundary layer and interior. In the Ekman layer, the $O(\epsilon)$ down-wind velocity can be related to the stream function using (4.15)

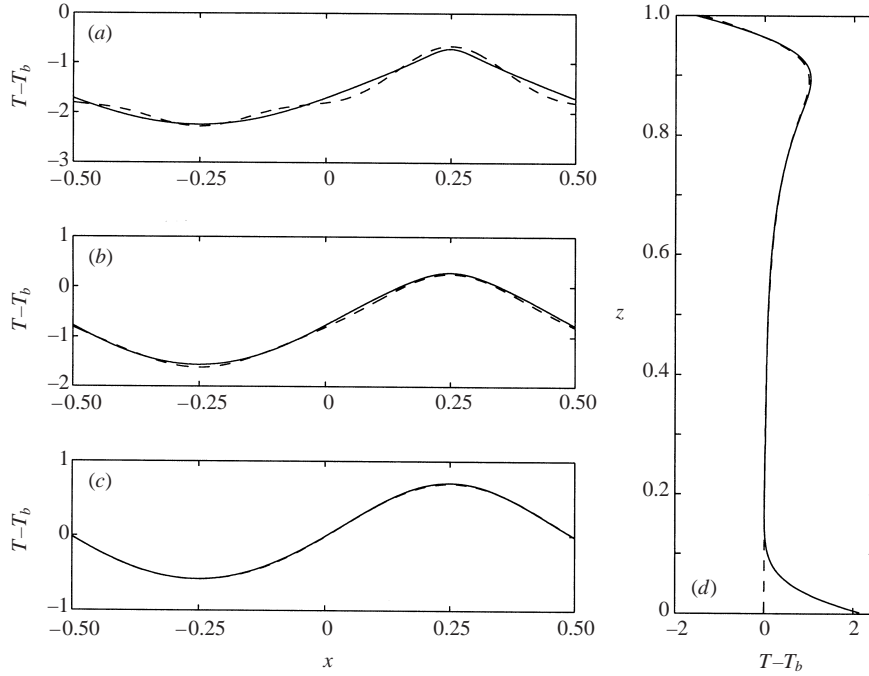


FIGURE 10. Same as figure 5 but for the nonlinear SSU solution for $T - T_b$ valid to $O(\epsilon)$, i.e. $T^{(3)} \equiv \epsilon^{-1/2} T_T^{(0)} + T_T^{(1)} + T_i^{(0)} + \epsilon^{1/2} T_T^{(2)} + \epsilon(T_T^{(3)} + T_i^{(2)} + T_e^{(2)})$. At this order, the unequal strength of downwelling and upwelling affects the solution.

and (3.4):

$$v_e^{(2)} = F_x + \frac{1}{2} \frac{\partial^3 \psi_e^{(2)}}{\partial \eta^3}. \quad (4.50)$$

In the thermal boundary layer, at this order the thermal-wind relation still holds:

$$\frac{1}{\gamma^{1/2}} \frac{\partial v_T^{(1)}}{\partial \xi} = - \frac{\partial T_T^{(2)}}{\partial x}. \quad (4.51)$$

Likewise, $v_i^{(2)}$ satisfies the thermal-wind balance:

$$\frac{\partial v_i^{(2)}}{\partial z} = \frac{\partial T_i^{(2)}}{\partial x}. \quad (4.52)$$

After vertically integrating (4.51) and (4.52), we have all the $O(\epsilon)$ corrections to the down-wind velocity. The lateral structure of the analytical solution for the down-wind velocity to $O(\epsilon)$, $v^{(2)} \equiv v_e^{(0)} + v_i^{(0)} + \epsilon^{1/2} v_T^{(0)} + \epsilon(v_e^{(2)} + v_i^{(2)} + v_T^{(1)})$, agrees well with the numerical solution, demonstrating the steepening (flattening) of v to the right (left) of $x = 0$ (figure 11). A result of this steepening/flattening is that the vertical component of the vorticity $\zeta^{(2)} = \partial v^{(2)} / \partial x$, plotted in figure 12, adopts an uneven distribution, with anticyclonic maxima being larger than cyclonic ones. This asymmetry can be seen in the vertical profiles of $\zeta^{(2)}$ evaluated at $x = 0.25$ and $x = -0.25$ shown in figure 12(d), which are not mirror images of each other except deep in the fluid. This uneven vorticity distribution is due to the asymmetric way in which the Ekman transport is modified in cyclonic versus anticyclonic regions. As is evident from (4.24) the Ekman transport is reduced in regions where the vorticity is cyclonic and enhanced where it

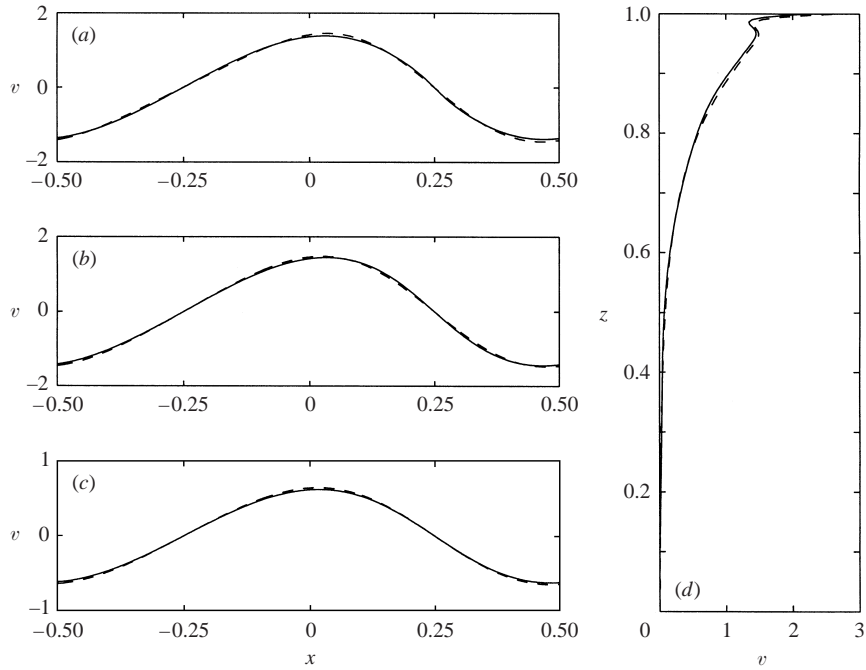


FIGURE 11. Same as figure 6 but for the nonlinear SSU solution for the down-wind velocity valid to $O(\epsilon)$, i.e. $v^{(2)} \equiv v_e^{(0)} + v_i^{(0)} + \epsilon^{1/2}v_T^{(0)} + \epsilon(v_e^{(2)} + v_i^{(2)} + v_T^{(1)})$.

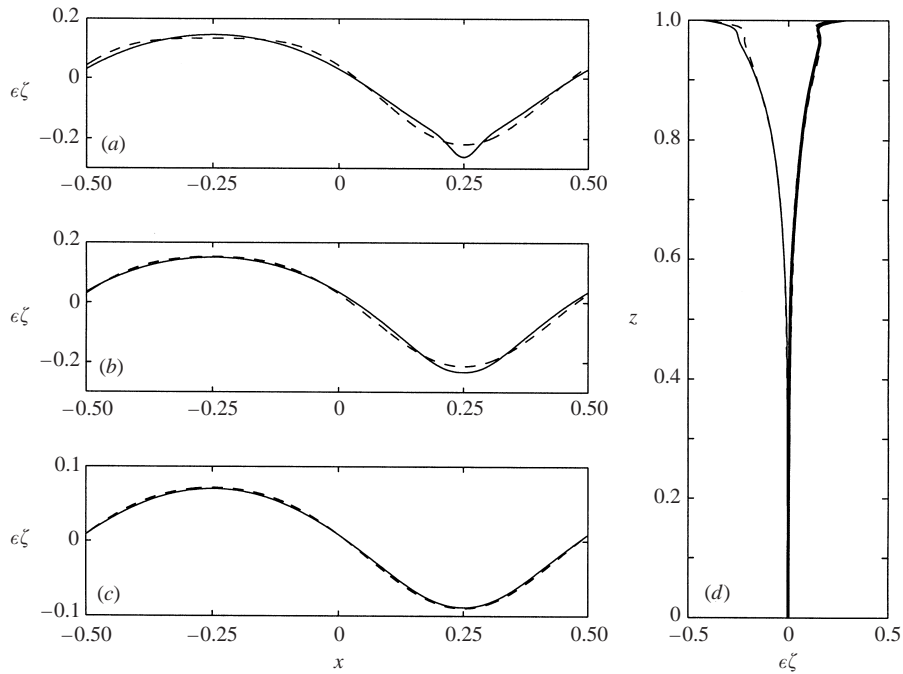


FIGURE 12. The nonlinear SSU solution for the vertical vorticity ζ valid to $O(\epsilon)$ (dashed) $\zeta^{(2)} = \partial v^{(2)} / \partial x$ compared to the numerical solution (solid) for $t = 0.31$. Both solutions are normalized by f . The lateral structure of ζ is plotted for (a) $z = 0.982$, (b) $z = 0.955$, and (c) $z = 0.815$. (d) Vertical profiles of ζ at $x = 0.25$ (thin solid and dashed lines) and $x = -0.25$ (thick solid and dashed lines).

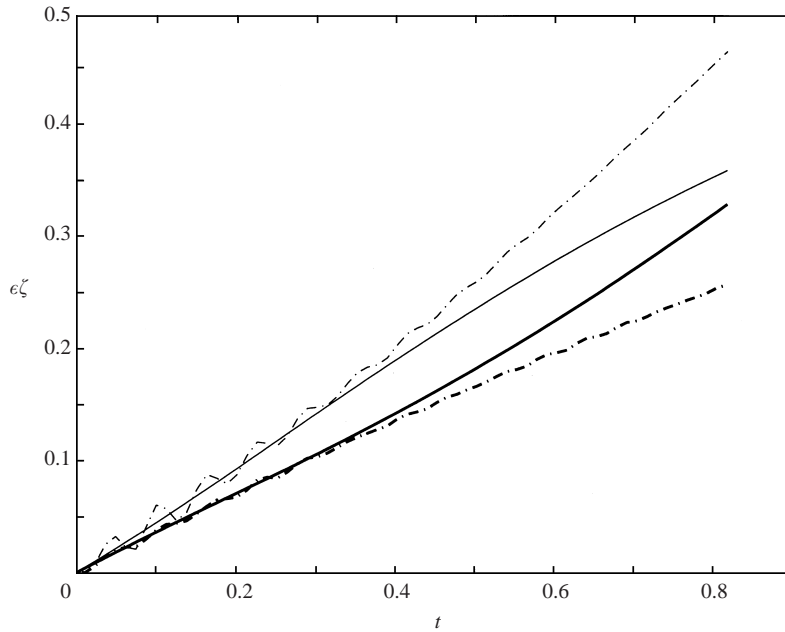


FIGURE 13. Time-series of the magnitude of the maximum anticyclonic vorticity at $x = 0.25$ (solid and dash-dotted thin lines) and the maximum cyclonic vorticity at $x = -0.25$ (solid and dash-dotted thick lines). The solid (dash-dotted) curves represent the nonlinear SSU (numerical) solutions. All vorticities are calculated at $z = 0.893$ and are normalized by f .

is anticyclonic. For this spin-up problem, anticyclonic (cyclonic) vorticity is generated where the Ekman transport is convergent (divergent). Since convergence of the Ekman transport is correlated with anticyclonic vorticity, by including nonlinearities, Ekman convergence will be stronger than divergence. This causes the anticyclonic vorticity to grow faster than the cyclonic vorticity (see figure 13), leading to the uneven vorticity distribution. In figure 13, plotted with the analytic solution for the time-series of the magnitude of the anticyclonic (cyclonic) vorticity at the location of the minimum (maximum) wind-stress curl is the corresponding unfiltered time-series from the numerical experiment. The trends of the unfiltered time-series are predicted well by the theory.

Preferential acceleration of anticyclonic vorticity by Ekman pumping/suction modified by the interior vertical vorticity is a result of horizontal advection of momentum in the Ekman layer. How does horizontal advection of temperature by Ekman flow affect the down-wind velocity and vertical vorticity? To answer this question, the $O(\epsilon)$ down-wind velocity in the thermal boundary layer associated with the horizontal advection of temperature by Ekman flow, v_{HADVT} , was calculated by substituting the HADVT term of (4.38) into the thermal-wind balance (4.51) and vertically integrating, resulting in

$$v_{\text{HADVT}} = 64\pi^3 S t^2 i^4 \operatorname{erfc}\left(\frac{\xi}{\sqrt{2t}}\right) \sin(4\pi x), \quad (4.53)$$

where

$$i^4 \operatorname{erfc}(\xi/\sqrt{2t}) = \int_{\xi/\sqrt{2t}}^{\infty} i^3 \operatorname{erfc}(s) ds.$$

When added to the total down-wind velocity, v_{HADVT} steepens the lateral profile of

v to the right of $x = 0$. The physical reason for why this is so is as follows. As mentioned in §4.7, horizontal advection of temperature by Ekman flow acts like an effective heat flux at the top of the thermal boundary layer. For the stratified spin-up problem, this heat flux always tends to cool the thermal boundary layer, with maximal cooling at the locations of the maximum and minimum wind stress where both the Ekman transport and lateral temperature gradients are largest. Where the wind-stress curl is negative, this cooling is in opposition to warming caused by downwelling, whereas in regions of positive wind-stress curl, the cooling augments cooling attributable to upwelling. Since cooling associated with horizontal advection of temperature by Ekman flow is displaced laterally from the centres of upwelling and downwelling, the net result is to intensify (weaken) the magnitude of horizontal density gradients, which in turn increases (reduces) the speed of the down-wind flow, in regions of negative (positive) wind-stress curl. Notice that while this mechanism for steepening of the down-wind velocity is of thermodynamic origin, it acts to reinforce the asymmetric vorticity distribution of stronger anticyclonic versus cyclonic vorticity caused by nonlinear Ekman pumping.

4.9. Breakdown of nonlinear stratified spin-up theory

As evident in figure 13, the numerical and analytical solutions of the vertical vorticity begin to diverge after $t \sim 0.4$. The same is true for the stream function, i.e. see figure 8(c), and the temperature field (compare figure 1c and figure 1i). Since the analytical solutions for all of the flow variables begin to fail after $t \sim 0.4$, it can be concluded that this behaviour signifies the limitation of the regular perturbation expansion to $O(\epsilon)$. To extend the time-period of validity for the expansion, the expansion could be carried out to higher orders in the Rossby number. To illustrate this point, we have calculated the stream function to $O(\epsilon^{3/2})$: $\psi^{(3)} \equiv \psi_e^{(0)} + \psi_i^{(0)} + \epsilon(\psi_e^{(2)} + \psi_i^{(2)} + \psi_T^{(0)}) + \epsilon^{3/2}(\psi_e^{(3)} + \psi_i^{(3)} + \psi_T^{(1)})$. The details of this calculation have been left out for brevity. The time-series of the vertical velocity at $x = -0.218$ demonstrates the anticipated result that the vertical velocity expanded to $O(\epsilon^{3/2})$ does better at predicting the temporal behaviour of the numerical solution with inertial oscillations filtered out (figure 14a). This is not true at $x = 0.218$ (figure 14b), where the vertical velocity of the numerical solution diverges rapidly from both the $O(\epsilon)$ and $O(\epsilon^{3/2})$ analytic solutions towards the end of the time-series. We will show in the next section that this strong downwelling at $x = 0.218$ is a manifestation of a hydrodynamic instability that arises as the potential vorticity of the fluid becomes negative. Evidently, nonlinear stratified spin-up theory, regardless of to what order of Rossby number the regular perturbation expansion is truncated at, is incapable of capturing the dynamics of a rapidly growing instability. Hence, the onset of instability marks the true breakdown of the theory.

4.10. Generation of negative potential vorticity and symmetric instability for late times

The spatial structure of the hydrodynamic instability responsible for the strong downwelling evident in the time-series shown in figure 14 is highlighted by the deviation of the stream function from the nonlinear stratified spin-up solution $\psi^{(3)}$ (figure 15). Two such instabilities form, and are centred about the strongest horizontal thermal gradients of the domain. Although the instabilities form where the static stability is unstable, they do not form where the density inversions are strongest, where gravitational instability is most likely to occur. The shaded area in the figure denotes a region where the absolute vorticity is negative and hence is a region prone

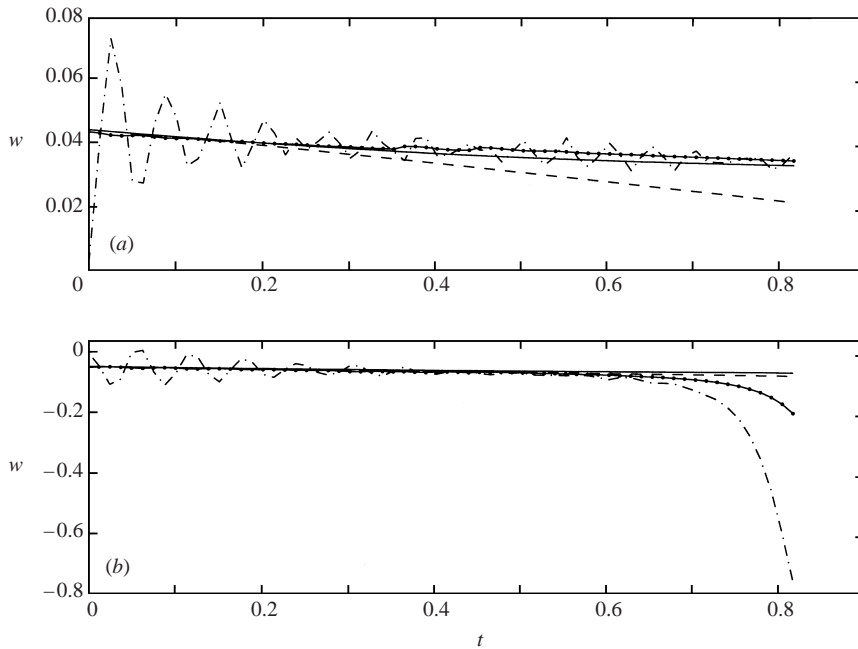


FIGURE 14. Time-series of the nonlinear SSU solution for vertical velocity valid to $O(\epsilon^{3/2})$, i.e. $-\partial\psi^{(3)}/\partial x$, and $O(\epsilon)$, i.e. $-\partial\psi^{(2)}/\partial x$ (solid and dashed lines respectively), along with the unfiltered (dash-dotted) and filtered (dots) numerical solutions evaluated at $z = 0.953$ and $x = -0.218$ (a) and $x = 0.218$ (b).

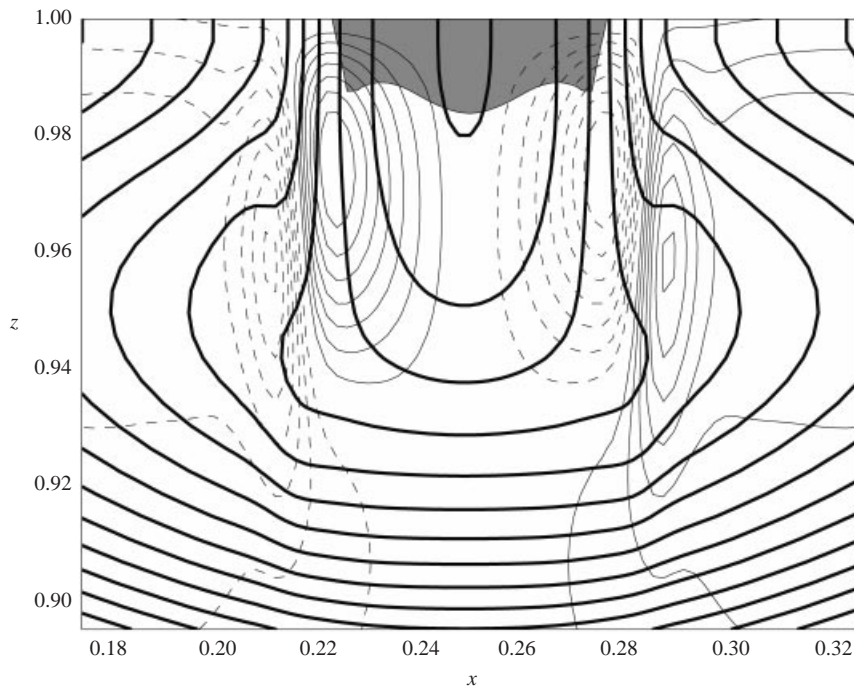


FIGURE 15. Spatial structure of symmetric instability. The numerical solution for the temperature (solid thick) and the deviation of the stream function from the nonlinear SSU solution (thin solid and dashed, where dashed contours indicate negative values) for $t = 0.82$. Shaded area indicates the region where the absolute vorticity is negative.

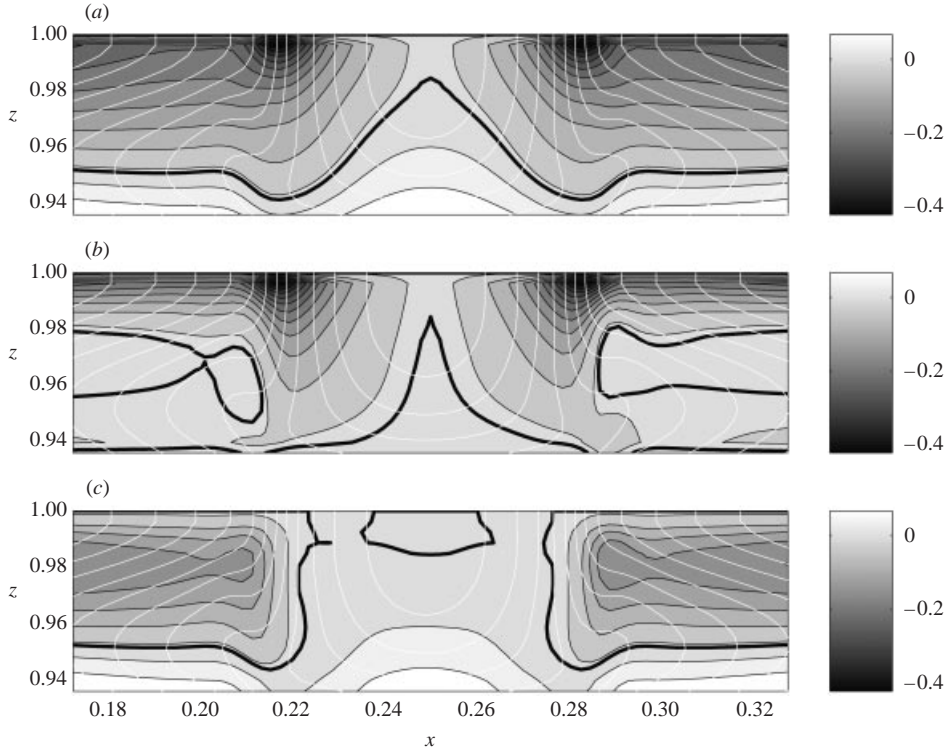


FIGURE 16. Potential vorticity and its constituent normalized by fN^2/g for $t = 0.82$. (a) The total potential vorticity. (b) The HORIZ term of the potential vorticity. (c) The VERT term of the potential vorticity. See equation (4.54) for the definitions of the terms HORIZ and VERT. Negative regions are enclosed by the thick black contour. Isotherms are contoured in white.

to inertial instability. Notice that the instabilities do not originate from this region either. This indicates that the disturbances found near the minimum wind-stress curl are neither gravitational nor inertial instabilities. Insight into the nature of inviscid two-dimensional instabilities occurring in rotating stratified fluids can be gained by computing the potential vorticity:

$$\Pi^* = \underbrace{\alpha \left(f + \frac{\partial v^*}{\partial x^*} \right) \frac{\partial T^*}{\partial z^*}}_{\text{VERT}} - \underbrace{\alpha \frac{\partial v^*}{\partial z^*} \frac{\partial T^*}{\partial x^*}}_{\text{HORIZ}}, \quad (4.54)$$

where the superscript * denotes a dimensional variable and the temperature in (4.54) includes the background temperature field. Hoskins (1974) showed that the necessary condition for instability for an inviscid rotating stratified fluid with no variation in one spatial dimension is that the potential vorticity must be negative. The potential vorticity can be made negative in several ways. The VERT term of the potential vorticity is negative if either the absolute vorticity is negative or the stratification is unstable. As mentioned before, if the absolute vorticity is less than zero then the fluid is prone to inertial instability, while unstable density gradients lead to gravitational instability. The HORIZ term of the potential vorticity for a flow in a thermal-wind balance is $-(\alpha g/f)(\partial T^*/\partial x^*)^2$, which is always negative and large in magnitude for intense thermal gradients. If the potential vorticity is made negative predominantly

by the HORIZ term, the ensuing disturbance is classified as symmetric instability. The most extremely negative areas of the total potential vorticity are concentrated near the sharpest density gradients found at $x = 0.22$ and 0.28 (figure 16*a*). Not surprisingly, the source of these extremely negative areas is the HORIZ term, which is plotted in figure 16*b*). The VERT term of the potential vorticity is displayed in figure 16*c*) and is negative where there are density inversions and where the absolute vorticity is negative. At the location of the minimum potential vorticity, the VERT term is negative but only constitutes 1% of the total. Since the potential vorticity is made negative predominately by the HORIZ term, we can conclude that the overturning cells shown in figure 15 are manifestations of symmetric instability. Having classified the disturbance, the next step will be to investigate the life cycle of the stratified spin-up process after the onset of symmetric instability.

5. Conclusions

Using both a weakly nonlinear analytic theory and direct numerical simulation, we have thoroughly documented all the processes involved during the spin-up of a rotating stratified fluid driven by moderately strong wind-stress forcing for time periods of order a homogeneous spin-up time. By moderately strong wind stress forcing we refer to winds with horizontal length scales of order the oceanic Rossby radius of deformation (making the Burger number S order-one) and of sufficient magnitude such that the Rossby number based on the wind forcing $\epsilon = \tau_o / \rho_o f^2 L \delta_e$ is not negligible or, more specifically, when the Rossby number is proportional to the square root of the Ekman number: $\epsilon \propto E^{1/2}$. We have also implemented a heat-flux rather than fixed-temperature boundary condition on the temperature field, which is more realistic for the ocean. To emphasize the role of mechanical versus buoyancy forcing on the spin-up process, a zero-heat-flux boundary condition was used. Our analysis reveals that the spin-up process, subject to the criteria listed above, differs from the classic linear view of SSU mainly in two ways: first, Ekman transport, which drives SSU, is not merely proportional to the wind stress, but is distorted by the flow generated during SSU, and second, strict application of the zero-heat-flux boundary condition leads to the growth of a diffusive thermal boundary layer of thickness $\delta_T = HE^{1/4}$ in which the stratification is reduced, the effects of horizontal advection of temperature by the flow in the Ekman layer are felt, and in which the secondary circulation and down-wind flow are modified.

The Ekman transport valid to $O(\epsilon)$ (equation (4.24)) differs from the classic formula by three terms. The first term reflects the fact that, as first pointed out by Stern (1965) and Niiler (1969), the Ekman transport varies inversely with the absolute vorticity rather than the planetary vorticity. As vertical relative vorticity is generated during the spin-up of the fluid by the secondary circulation, the vertical shear of the flow in the Ekman layer tilts lines of absolute vorticity away from the vertical to replenish frictional twisting of vorticity. Because the shear tilts absolute rather than planetary vorticity, the Ekman transport is enhanced in regions of anticyclonic vorticity so that the tilting of the diminished absolute vorticity can balance the dissipation. This effect causes Ekman pumping to be stronger than Ekman suction because it is correlated with anticyclonic vorticity. The second term in the Ekman transport formula is steady in time and is attributable to vertical and horizontal advection of the momentum of the flow in the Ekman layer. Although the secular growth of the vertical vorticity term eventually overwhelms the effect of this steady term, for early times the steady term dominates, again enhancing Ekman pumping and reducing Ekman suction. The flow

in the Ekman layer is driven by stress at the surface of the fluid. For wind-driven SSU, wind shear provides this stress. During SSU, the secondary circulation accelerates a geostrophic flow with shear in the same direction as the wind stress. At the surface, this geostrophic shear partially compensates for the wind shear and therefore reduces the force driving the cross-wind flow in the Ekman layer. The amount by which Ekman transport is reduced by this mechanism is given by the last term in (4.24).

As the Ekman transport is distorted by the flow generated during SSU, the interior secondary circulation adjusts accordingly. By the vorticity effect, interior downwelling is stronger than upwelling, which, through the process of vortex stretching, favours the generation of anticyclonic over cyclonic vorticity. Hence, a feedback mechanism is apparent: anticyclonic vorticity enhances Ekman pumping which intensifies vortex squashing and strengthens anticyclonic vorticity, while cyclonic vorticity reduces Ekman suction which weakens vortex stretching and diminishes cyclonic vorticity. Through this mechanism the initial sinusoidal profile of the down-wind velocity is steepened, see figure 11. Notice that this steepening does not rely on nonlinear advection in the interior. This contrasts with a model for nonlinear barotropic spin-down proposed by Zavala Sansón & van Heijst (2000) in which stretching and horizontal advection of interior relative vertical vorticity by frictionally induced secondary circulation causes cyclonic vortices to spin down faster than anticyclonic vortices. While these nonlinear vorticity generation mechanisms are present in stratified spin-up, vertical advection and tilting of the x -component of the vorticity to the vertical (vorticity generation mechanisms which require vertical variation of the geostrophic flow and hence are absent in barotropic spin-down) are active in SSU and nearly cancel stretching and horizontal advection of interior vertical vorticity when the Burger number is of order-one. On account of this, we conclude that the dynamics in the interior of the fluid, at least during the early stages of SSU, are predominantly linear, driven by Ekman pumping modified by nonlinearity in the Ekman layer.

At the surface and base of the fluid the initial stratification does not satisfy the zero-heat-flux boundary condition. Consequently, near these horizontal boundaries, diffusion reduces the stratification, creating thermal boundary layers which, for time periods of order a homogeneous spin-up time, have a thickness $\delta_T = HE^{1/4}$. In this way the fluid naturally generates a surface mixed layer $E^{-1/4}$ times thicker than the Ekman layer embedded within it. In the Ekman layer, cross-wind flow advects cool upwelled water towards warmer downwelled water. This horizontal advection of temperature, which tends to cool the fluid, is balanced by vertical diffusion of heat. Diffusion in the Ekman layer extracts heat from the thermal boundary layer beneath so as to counteract this cooling tendency. The flux of heat extracted from the top of the thermal boundary layer by this mechanism (in dimensional units, i.e. W m^{-2}) is

$$\text{QADV}^* = \rho_o c_p M \frac{\partial T_s^*}{\partial x^*}, \quad (5.1)$$

where the superscript $*$ denotes a dimensional variable, c_p is the specific heat of water, M is the Ekman transport, and T_s^* is the sea-surface temperature. The thermodynamic response of the thermal boundary layer to the heat flux (5.1) is nearly identical to that of surface cooling imposed by an external source (say evaporative cooling for example), i.e. its signal diffuses down into the fluid. The difference being due to the dependence of (5.1) on the sea-surface temperature, QADV^* relies on the internal dynamics of the fluid which is determined by the SSU process. This coupling between the internal dynamics of the fluid and the heat-flux boundary condition leads to an asymmetry in the magnitude of lateral density gradients in regions of downwelling

versus upwelling. In regions of downwelling (upwelling) the cooling associated with (5.1) counteracts (augments) the warming (cooling) driven by the downwelling (upwelling). Since the maximal cooling of QADV* is displaced horizontally from the centres of upwelling and downwelling, the cooling enhances (reduces) the magnitude of lateral density gradients in regions of downwelling (upwelling). Down-wind flow in the thermal boundary layer is geostrophic; therefore, following the thermal-wind relation, the maximum magnitudes of the geostrophic shear as well as the down-wind flow are shifted towards the centre of downwelling on account of QADV*. This thermodynamic process makes anticyclonic vorticity stronger than cyclonic vorticity, similar to the result caused by nonlinear Ekman pumping. At the same time, the increased horizontal temperature gradients and ensuing geostrophic shear in the region of Ekman convergence reduces the potential vorticity to negative values and conditions the fluid for symmetric instability. Onset of symmetric instability marks the breakdown of nonlinear SSU theory and the beginning of the next phase in the stratified spin-up life cycle during which overturning instabilities and frontogenesis are prominent. We are currently investigating this later phase.

The effects described in this paper of the modification of the SSU process by nonlinear corrections to the Ekman pumping occur most rapidly for large Rossby and Burger numbers. The f^{-2} dependence of both of these numbers suggests that the low latitudes are particularly susceptible to the dynamics of nonlinear SSU. We present an example where this appears to be the case. In the tropical Pacific off the coast of Central America, the ocean is strongly forced by wind jets funnelled through gaps in the mountain ranges found in the region, Kessler (2002). Nine-month-averaged NSCAT scatterometer winds (Milliff & Morzel 2001), as well as *in situ* shipboard wind data (Trasviña *et al.* 1995), show that the jets force the ocean with nearly equal amounts of positive and negative wind-stress curl. Despite the symmetry of the forcing, the ocean's response is quite asymmetrical, characterized by intense anticyclonic warm-core eddies generated to the right of the axis of the wind jet and weaker cyclonic eddies to the left, (Barton *et al.* 1993; Trasviña *et al.* 1995). Based on the nine-month-averaged scatterometer winds (Milliff & Morzel 2001), the wind jets yield wind-stress curls of order $3.5 \times 10^{-7} \text{ N m}^{-3}$. Using an Ekman depth δ_e of 25 m (Kessler 2002), the Rossby number of this flow is estimated to be: $\epsilon = 3.5 \times 10^{-7} \text{ N m}^{-3} / [(1024 \text{ kg m}^{-3})(3.5 \times 10^{-5} \text{ s}^{-1})^2(25 \text{ m})] = O(0.01)$. This calculation is based on averaged winds; Rossby numbers for individual wind events are likely to be much larger. The width of the wind jet (200 km) is determined by the size of the gap in the mountain range through which it flows (Trasviña *et al.* 1995). The Rossby radius of deformation in this part of the Pacific ocean is $\sim 200 \text{ km}$, and therefore the Burger number S of these flows is order-one. Since these values of ϵ and S are of the same order as the parameters used in this study ($\epsilon = 0.02$ and $S = 1$) we hypothesize that the dominance of anticyclonic over cyclonic eddies in this region is attributable to our proposed feedback mechanism in which anticyclonic vorticity enhances Ekman pumping, intensifies vortex squashing, and thus preferentially generates anticyclonic vorticity.

This work was supported by the National Science Foundation, Physical Oceanography Program.

REFERENCES

- ABRAMOWITZ, M. & STEGUN, I. 1972 *Handbook of Mathematical Functions*. Wiley Interscience.
 ALLEN, J. S. 1973 Upwelling and coastal jets in a continuously stratified ocean. *J. Phys. Oceanogr.* **3**, 245–257.

- BARTON, E. D., ARGOTE, M. L., BROWN, J., KOSRO, P. M., LAVIN, M., ROBLES, J. M., SMITH, R. M., TRASVIÑA, A. & VELEX, H. S. 1993 Supersquirt: Dynamics of the Gulf of Tehuantepec, Mexico. *Oceanography* **6**, 23–30.
- BUZYNA, G. & VERONIS, G. 1971 Spin-up of a stratified fluid: theory and experiment. *J. Fluid Mech.* **50**, 579–608.
- GREENSPAN, H. & HOWARD, L. N. 1963 On a time-dependent motion of a rotating fluid. *J. Fluid Mech.* **17**, 385–404.
- HART, J. E. 2000 A note on nonlinear corrections to the Ekman layer pumping velocity. *Phys. Fluids* **12**, 131–135.
- HOLTON, J. R. 1965a The influence of viscous boundary layers on transient motions in a stratified rotating fluid: Part I. *J. Atmos. Sci.* **22**, 402–411.
- HOLTON, J. R. 1965b The influence of viscous boundary layers on transient motions in a stratified rotating fluid: Part II. *J. Atmos. Sci.* **22**, 535–540.
- HOSKINS, B. J. 1974 The role of potential vorticity in symmetric stability and instability. *Q. J. R. Met. Soc.* **100**, 480–482.
- KESSLER, W. S. 2002 Mean three-dimensional circulation in the northeast tropical Pacific. *J. Phys. Oceanogr.* **32**, 2457–2471.
- LEE, D., NIHLER, P., WARN-VARNAS, A. & PIACSEK, S. 1994 Wind-driven secondary circulation in ocean mesoscale. *J. Mar. Res.* **52**, 371–396.
- MILLIFF, R. F. & MORZEL, J. 2001 The global distribution of the time-average wind stress curl from NSCAT. *J. Atmos. Sci.* **58**, 109–131.
- NIHLER, P. 1969 On the Ekman divergence in an oceanic jet. *J. Geophys. Res.* **74**, 7048–7052.
- SAKURAI, T. 1969 Spin down problem of rotating stratified fluid in thermally insulated circular cylinders. *J. Fluid Mech.* **37**, 689–699.
- STERN, M. E. 1965 Interaction of a uniform wind stress with a geostrophic vortex. *Deep-Sea Res.* **12**, 355–367.
- TRASVIÑA, A., BARTON, E. D., BROWN, J., VELEX, H. S., KOSRO, P. M. & SMITH, R. L. 1995 Offshore wind forcing in the Gulf of Tehuantepec, Mexico: the asymmetric circulation. *J. Geophys. Res.* **100**(C10), 20649–20663.
- WALIN, G. 1969 Some aspects of time-dependent motion of a stratified rotating fluid. *J. Fluid Mech.* **36**, 289–307.
- ZAVALA SANSÓN, L. & VAN HEIJST, G. J. F. 2000 Nonlinear Ekman effects in rotating barotropic flows. *J. Fluid Mech.* **412**, 75–91.